AD_____

Award Number: W81XWH-09-1-0405

TITLE: Understanding Collagen Organization in Breast Tumors to Predict and Prevent Metastasis

PRINCIPAL INVESTIGATOR: Dr. Edward Brown

CONTRACTING ORGANIZATION: University of Rochester
Rochester, NY 14611

REPORT DATE: September 2011

TYPE OF REPORT: Annual

PREPARED FOR: U.S. Army Medical Research and Materiel Command
Fort Detrick, Maryland 21702-5012

REPORT DOCUMENTATION PAGE

Form Approved
OMB No. 0704-0188

1. REPORT DATE *(DD-MM-YYYY)*	2. REPORT TYPE	3. DATES COVERED *(From - To)*
01-09-2011	Annual	1 SEP 2010 - 31 AUG 2011

4. TITLE AND SUBTITLE
Understanding Collagen Organization in Breast Tumors to Predict and Prevent Metastasis

5a. CONTRACT NUMBER

5b. GRANT NUMBER
W81XWH-09-1-0405

5c. PROGRAM ELEMENT NUMBER

6. AUTHOR(S)
Dr. Edward Brown

E-Mail: edward_brown@urmc.rochester.edu

5d. PROJECT NUMBER

5e. TASK NUMBER

5f. WORK UNIT NUMBER

7. PERFORMING ORGANIZATION NAME(S) AND ADDRESS(ES)
University of Rochester
Rochester, NY 14611

8. PERFORMING ORGANIZATION REPORT NUMBER

9. SPONSORING / MONITORING AGENCY NAME(S) AND ADDRESS(ES)
U.S. Army Medical Research and Materiel Command
Fort Detrick, Maryland 21702-5012

10. SPONSOR/MONITOR'S ACRONYM(S)

11. SPONSOR/MONITOR'S REPORT NUMBER(S)

12. DISTRIBUTION / AVAILABILITY STATEMENT
Approved for Public Release; Distribution Unlimited

13. SUPPLEMENTARY NOTES

14. ABSTRACT
The ordering of collagen fibers within a tumor has significant influence on tumor metastasis. in murine breast tumor models, tumor cells move towards blood vessels along fibers that are visible via second harmonic generation (SHG), and SHG is exquisitely sensitive to molecular ordering. Tumor cells that are moving along SHG-producing (i.e. ordered) collagen fibers move significantly faster than those cells that are moving independently of SHG-producing fibers, and the extent of SHG-associated tumor cell motility is correlated with metastatic ability of the tumor model. Furthermore, the tumor-host interface of murine breast tumor models is characterized by radially oriented SHG-producing fibers associated with tumor cells invading the surrounding tissue. Consequently we believe that the process of establishing ordered fibers offers an exciting, and currently unexploited, therapeutic target. To take advantage of this, we must first learn the cellular players and molecular signals by which collagen ordering is induced. Therefore, in this application we propose to determine the key cells and signals which influence the ordering of collagen in breast tumors, determine if this ordering is predictive of metastasis, and develop new optical tools to study this ordering.

15. SUBJECT TERMS
Microscopy, metastasis

16. SECURITY CLASSIFICATION OF:			17. LIMITATION OF ABSTRACT	18. NUMBER OF PAGES	19a. NAME OF RESPONSIBLE PERSON
a. REPORT	b. ABSTRACT	c. THIS PAGE			USAMRMC
U	U	U	UU	48	19b. TELEPHONE NUMBER *(include area code)*

Table of Contents

Introduction……..…….....4

Body…….5

Key Research Accomplishments……..…….……9

Reportable Outcomes……...…….9

Conclusions……...……..9

Appendices……10

Introduction.

The extent and nature of the ordering of collagen fibers within a tumor has significant influence on the process of tumor metastasis: in murine breast tumor models, tumor cells move towards blood vessels along fibers that are visible via second harmonic generation (SHG), and SHG is exquisitely sensitive to molecular ordering (see below). Tumor cells that are moving along SHG-producing (i.e. ordered) collagen fibers move significantly faster than those cells that are moving independently of SHG-producing fibers, and the extent of SHG-associated tumor cell motility is correlated with metastatic ability of the tumor model. Furthermore, the tumor-host interface of murine breast tumor models is characterized by radially oriented SHG-producing fibers associated with tumor cells invading the surrounding tissue. Lastly, we have shown that treatment of tumors with the hormone relaxin, known to alter metastatic ability, alters the collagen ordering as detectable by SHG.

As locomotion along ordered (SHG-producing) fibers plays a pivotal role in the metastatic process, we believe that the process of establishing ordered fibers offers an exciting, and currently unexploited, therapeutic target. To take advantage of this, we must first learn the cellular players and molecular signals by which collagen ordering is induced. Therefore, in this application we propose to *determine the key cells and signals which influence the ordering of collagen in breast tumors*. We will do this by disrupting candidate cells and signals in mouse models of breast cancer using SHG-based measures of collagen ordering, and metastasis, as readouts. Additionally, we will *determine if SHG measures of collagen ordering in breast tumors are clinically useful predictors of metastatic outcome in breast cancer patient biopsies*.

This work will have great impact for several reasons. It will provide important insight into the molecular and cellular mechanisms by which the collagen in breast tumors is ordered, and how this ordering affects metastatic ability. In future work we can then exploit these findings by developing and evaluating clinically useful therapeutic techniques that will target, for the first time, the ordering of tumor collagen and hence attempt to inhibit metastatic ability, improving patient survival. This project will also explore whether collagen ordering in the tumor, as quantified by SHG, is a clinically viable predictor of metastatic outcome in patient biopsies. A measure of metastatic ability is extremely exciting, because there is currently an identified, pressing need for patient stratification based upon metastatic risk, in order to minimize 'over treatment' of patients who only require local therapy after resection, not systemic chemotherapy[6]. This would improve patients' quality of life. Hence, this project has promise to be clinically relevant through two separate paths.

Body

The Statement of Work for this grant proposal is as follows:

Statement of Work

Specific Aim 1. Determine the role of macrophages in governing collagen ordering in tumors, and their mechanism of action. (Months 1-30)

1a) Modulate the presence of macrophages, then evaluate the effects on collagen ordering in tumors, and the effects on metastatic burden. (Months 1-12) Uses liposome treatment. ~50 mice. Verifies involvement of macrophages' in collagen ordering in tumors, the exact nature of their particular impact on collagen ordering, and the impact on metastasis.

1b) Manipulate the expression of candidate genes in macrophages, and evaluate the effects on collagen ordering in tumors, and the effects on metastatic burden (Months 13-30) Uses bone marrow transfer after irradiation. Source animals are one of 7 knockouts, for 7 candidate genes. ~50x7= 350 mice. Produces identity of key signaling molecules involved in collagen ordering in tumors, the exact nature of their particular impact on collagen ordering, and the impact on metastasis.

Specific Aim 2. Determine the role of Th1, Th2, and Tregs in governing collagen ordering in tumors, and their mechanism of action. (Months 31-60)

2a) Modulate the presence of each cell type, then evaluate the effects on collagen ordering in tumors, and the effects on metastatic burden.(Months 31-42) Uses cell transfer after antibody treatment. ~3x50=150 mice. Produces identity of key cells involved in collagen ordering in tumors, the exact nature of their particular impact on collagen ordering, and the impact on metastasis.

2b) Manipulate the expression of candidate genes in those cell types found significant in 2a, and evaluate the effects on collagen ordering in tumors, and the effects on metastatic burden (Months 43-60) Uses cell transfer after antibody treatment. Source animals are one of 7 knockouts, for 7 candidate genes. ~3x50x7=1050 mice. Produces identity of key signaling molecules involved in collagen ordering in tumors, the exact nature of their particular impact on collagen ordering, and the impact on metastasis.

Specific Aim 3. Determine if collagen ordering is a clinically useful predictor of metastatic ability in human tissue samples (Months 1-60).

1a) In archival specimens from breast tumors we will evaluate the predictive relationships between collagen ordering and metastatic outcome (Months 1-60). Uses pathology samples of 4 breast tumor types to determine if SHG can predict metastatic outcome. ~4x50=200 samples. Produces an assessment of SHG's predictive ability.

We have concentrated on developing, proving, and utilizing the molecular tools required to manipulate macrophage populations in the E0771 tumor model in order to advance the goals of Specific Aim 1, while also establishing the staining and quantification regimen required to determine an optical "order index" or OI, which is required to advance the goals of all three specific aims.

As a result, we have completed a key manuscript, which we have recently submitted for publication, which essentially completes Aim 1 by determining that tumor associated macrophages are key players in establishing collagen ordering, that they operate through expression of TNF-α, and that alterations in collagen ordering via manipulation of macrophages or TNF-α is correlated with metastatic output. I will summarize the key steps of this work, and it is also appended to this document.

In that manuscript we first demonstrate that E0771 breast cancer cells do not produce significant TNF-α cells *in vitro* (Figure 1), while RAW264.7, a transformed murine macrophage line, does produce TNF-α, as do cells separated from E0771 tumors using magnetic beads loaded with antibodies against CD11b (a surface marker for cells of myeloid origin and presumably including tumor associated macrophages, or TAMs). Next we demonstrate that TNF-α is present in E0771 tumors grown in C57Bl/6 mice, but not mice lacking TNF-α, indicating the E0771 cell line does not alter its TNF-α expression capability *in vivo* (Figure 2). Next we determined that E0771 does not respond by proliferating or apoptosing to TNF-α *in vitro* (Figure 3). This is

unlike the T47D and MCF-7 cell lines, which as shown in the literature respond to TNF-α by proliferating and apoptosing, respectively. Next, we showed that proliferation of macrophages *in vitro* is significantly and specifically impeded by clodronate liposome (ClodL) therapy relative to control PBSL therapy, but proliferation of fibroblasts and cancer cells is unaffected (Figure 4).

The remaining results focus on the response of the tumor extracellular matrix to the manipulations of TAMs and stromal TNF-α which were characterized in the previous paragraph. We grew E0771 tumors over the course of three weeks, in wildtype or TNF–$\alpha^{-/-}$ mice, and in the presence or absence of chronic TAM depletion vial ClodL therapy. We then sacrificed, sectioned and stained the tumors with fluorescently labeled anti-collagen antibodies. Next we imaged the sections with second harmonic generation (SHG) a nonlinear light scattering interaction that is sensitive to overall collagen content at the laser focus, as well as fibril diameter, spacing, and order versus disorder in fibril packing. As shown in Figure 5, tumors grown in wildtype mice with no TAM depletion had statistically significantly greater SHG signal than tumors grown in wildtype mice with TAM depletion, as well as tumors grown in TNF-$\alpha^{-/-}$ mice both with and without TAM depletion. Additionally tumors grown in wildtype mice with TAM depletion had statistically significantly less SHG signal than tumors grown in TNF-$\alpha^{-/-}$ mice without TAM depletion. SHG is sensitive both to structural properties of collagen (fibril diameter, spacing, order) as well as to simple collagen content, so we also quantified anti-collagen antibody stain. As shown in Figure 6, tumors grown in wildtype mice with no TAM depletion had statistically significantly lesser fluorescence signal than tumors grown in wildtype mice with TAM depletion, as well as tumors grown in TNF-$\alpha^{-/-}$ mice both with and without TAM depletion. Furthermore, tumors grown in TNF-$\alpha^{-/-}$ mice with no TAM depletion had statistically less staining than tumors grown in TNF-$\alpha^{-/-}$ mice with TAM depletion. Finally, in order to minimize the effects of simple changes in collagen content on our readouts, we defined the Order Index, or OI, which is simply the ration of SHG to antibody stain, and is a parameter primarily sensitive to changes in structural properties of collagen (fibril diameter, spacing, order) and relatively insensitive to simple changes in collagen content. As shown in Figure 7, tumors grown in wildtype mice with no TAM depletion had statistically significantly greater OI than tumors grown in wildtype mice with TAM depletion, as well as tumors grown in TNF-$\alpha^{-/-}$ mice both with and without TAM depletion. No other cohort was different from another.

We also investigated the metastatic output to the lungs after each of these manipulations, and as shown in Figure 8, tumors grown in wildtype mice with no TAM depletion had statistically significantly greater metastatic output than tumors grown in wildtype mice with TAM depletion, as well as tumors grown in TNF-$\alpha^{-/-}$ mice both with and without TAM depletion. No other cohort was different from another.

Taken together, these data suggest that in the E0771 model of metastatic breast cancer TAMs influence collagen structure (Figure 7, columns 1 and 2 are different), and that host TNF-α influences collagen structure (Figure 7, columns 1 and 3 are different). Furthermore it suggests that TAMs influence collagen structure through TNF-α expression, that there are no other significant parallel mechanisms by which TAMs act, and that there are no other significant host cell types utilizing TNF-α to influence collagen structure (Figure 7, columns 2, 3, and 4 are the same). However there are some hints that TAMs may also use a minor parallel pathway to influence collagen ordering independent of TNF-α (Figure 5, columns 2 and 3 are different, and more importantly Figure 6, columns 3 and 4 are different). In each case, alterations in OI correlate with alterations in metastatic output, suggesting that OI affects metastatic ability, or that the two phenomena have a common root cause.

Figures

Figure 1: E0771 breast cancer cells do not produce significant TNF-α *in vitro*. By comparison, unstimulated RAW264.7, a transformed murine macrophage cell line, produces easily detectable TNF-α both when unstimulated and upon activation with 100 ng/mL LPS for 24 hours. Furthermore, cells separated from E0771 tumors using magnetic antibodies against CD11b (a surface marker for cells of myeloid origin and presumably including TAMs) also produced significant levels of TNF-α *in vitro*. ELISA sensitivity 5.1 pg/mL, n = 8 samples for all but E0771/CD11b+, where n = 5. Both control (media only) and E0771 supernatants registered below sensitivity (not detectable).	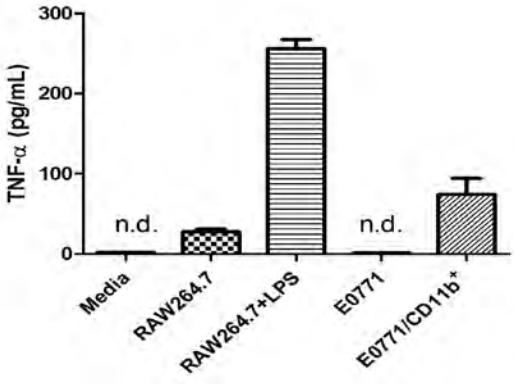
Figure 2: TNF-α is present in E0771 tumors grown in C57Bl/6 mice, but not mice lacking TNF-α indicating the E0771 cell line does not alter its TNF-α expression capability *in vivo*. TNF-α levels quantified by ELISA as in Figure 1. Total protein levels quantified by BCA assay (n =7 per group). TNF-α sensitivity 5.1 pg/mL, and TNF-α (-/-) lysates registered below sensitivity (not detectable).	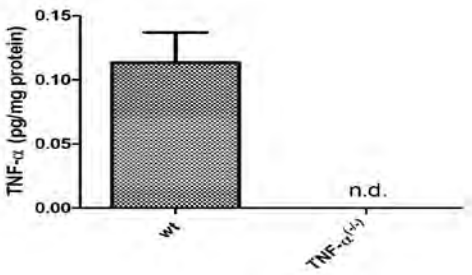
Figure 3: E0771 does not respond by proliferating or apoptosing to TNF-α *in vitro*. Proliferation presented as fluorescent intensity standardized to media-only control samples, n = 10 per group. Pairwise comparisons indicate T47D proliferation is significantly ($p<.01$) elevated by 20 ng/mL TNF-α at 48 hours, while MCF-7 experiences significant ($p<.05$) decreases in proliferation at the same dose over the same time course. E0771 shows no significant alteration in proliferation in response to this dose over this time course.	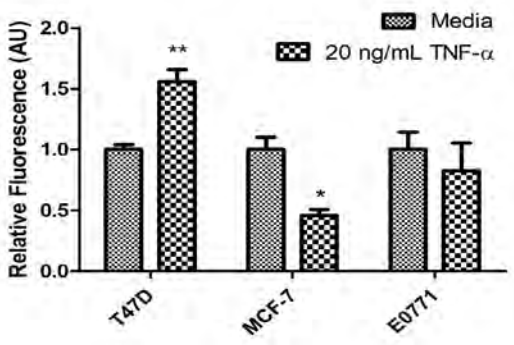
Figure 4: Proliferation of macrophages *in vitro* is significantly and specifically impeded by ClodL therapy relative to control PBSL therapy, but proliferation of fibroblasts and cancer cells is unaffected. Fluorescent intensities were standardized to the 0 mg/mL (media alone) condition for each group to account for differences in proliferative rate inherent in cell type. At all levels of ClodL, HFF-1 fibroblasts and E0771 breast cancer cells were unaffected and proliferated at a rate equivalent to those in PBSL, or in media alone. Only in the case of RAW264.7 macrophages did ClodL exert an anti-proliferative effect relative to PBSL controls, and did so in a roughly dose-dependent manner (n=8 each).	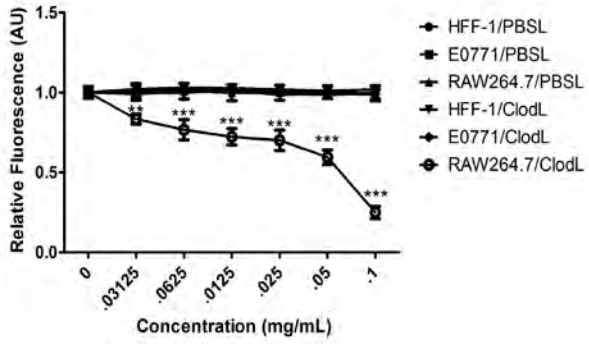

Figure 5: Effects of macrophage depletion and TNF-α deletion on SHG in the E0771 tumor. Average brightness of SHG-producing fibers declines as a result of TAM depletion, but not of TNF-α absence ($p<.0001$ and $p=.3122$ respectively). However, there is a high interaction between variables ($p=.0004$). A main effect is noticed ($p<.0001$). n = 21, 16, 15, and 15 from left. When Bonferroni post-hoc analysis is conducted, wildtype/PBSL mice show significantly elevated SHG compared to other groups, and wt/clodl treated tumors differ from TNF-α knockouts treated with PBS ($p<.05$). Note that SHG is sensitive to collagen structure and content, suggesting we should normalize for content separately with immunofluorescence (see Figure 7).	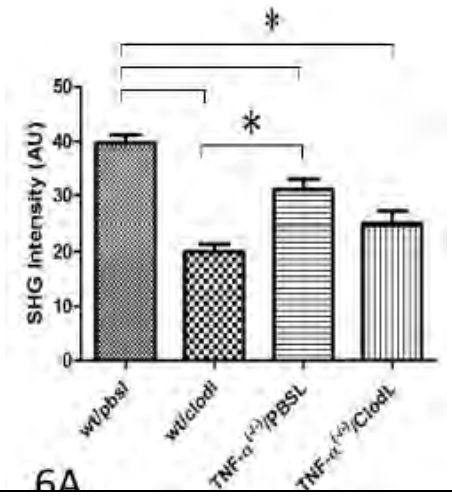
Figure 6: Effects of macrophage depletion and TNF-α deletion on collagen immunofluorescence (IF) in the E0771 tumor. Presence of tumor collagen as defined by average brightness of IF fibers increases as a result of both TAM depletion and TNF-α absence ($p<.0001$ both). However, there is a high interaction between variables ($p=.04$). A main effect is noticed ($p<.0001$). n = 21, 16, 15, and 15 from left. When Bonferroni post-hoc analysis is conducted, wildtype/PBSL mice show significantly decreased total collagen presence compared to other groups, and TNF-α knockouts treated with PBS differ from those treated with clodl ($p<.05$).	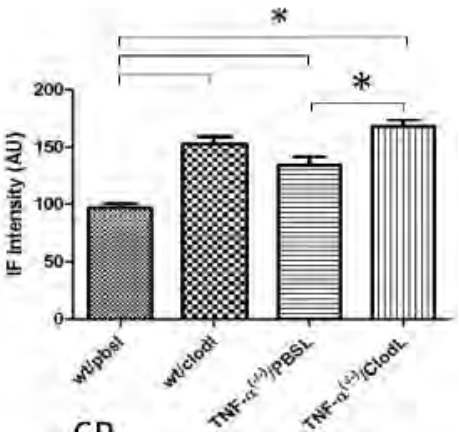
Figure 7: Effects of macrophage depletion and TNF-α deletion on collagen I structure relative to total collagen I presence in the E0771 tumor (OI). Both TAM depletion and TNF-α absence significantly decrease OI ($p<.0001$ and $p=.0130$ respectively). Again, a high interaction is present ($p=.0027$) and a main effect is noticed ($p<.0001$). Bonferroni post-hoc analysis shows wildtype/PBSL mice show significantly elevated OI relative to other treatment groups, but no other effects ($p<.05$).	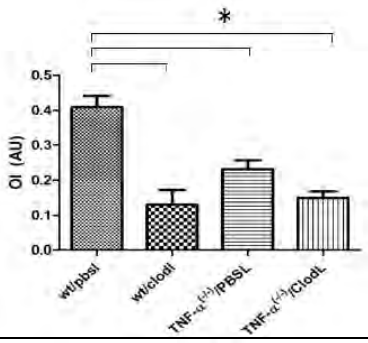
Figure 8: Lung metastatic burden decreases sharply with both macrophage depletion and TNF-α deletion. TAM depletion in wildtype mice results in significantly lower metastatic burden ($p<.001$) relative to control, whereas this effect disappears in TNF-α-deficient mice. Again, a high interaction is present ($p=.0007$) and a main effect is noticed ($p<.0001$). Bonferroni post-hoc analysis suggests that removing TNF-a results in significant ($p<.001$) decrease in metastatic events, as does depletion of TAMs, but that depletion of TAMs AND TNF-α causes no further decrease in metastatic burden ($p>.05$).	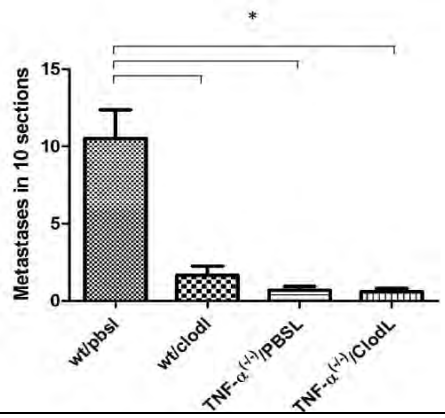

Key Research Accomplishments in the second year:

Used clodronate liposomes to ablate tumor associated macrophages *in vivo*, verified ablation, and found that this ablation affected the collagen ordering index (OI) as well as metastatic output.

Used clodronate liposomes to ablate tumor associated macrophages *in vivo*, in the presence and absence of TNF-a, and determined that this ablation also affected collagen ordering as well as metastatic output in a manner that indicated macrophage expression of TNF-a was the mechanism whereby OI was altered.

Reportable Outcomes:

Over the past year I published three papers based upon work funded all or in part by this award (note that Sullivan et al was reported last year as "Manuscript Submitted"):

Perry S, Norman J, Barbieri J, Brown E, Gelbard H. (2011) Mitochondrial membrane potential probes and the proton gradient: a practical usage guide. *BioTechniques.* 50(2): 98–115 [PMC3115691]

Sullivan K, Brown E. (2011) Diffusion and multi-photon fluorescence recovery after photobleaching in bounded systems. *Physical Review E*. 83(5): 051916 [http://link.aps.org/doi/10.1103/PhysRevE.83.051916]

Madden K, Szpunar M, Brown E. (2011) ß-adrenergic receptors regulate VEGF and IL-6 production by divergent pathways in high ß-AR-expressing breast cancer cell lines. *In Press, Breast Cancer Research and Treatment.* [PMC3126869]

I have also submitted one manuscript based upon work funded in whole or in part by this grant, and it is appended to this document:

Burke R, Madden K, Perry S, Zettel M, Brown E. (2011) Tumor-associated macrophages and stromal TNF-α play central roles in the regulation of collagen structure in breast tumor models as visualized by second harmonic generation. *Manuscript Submitted.*

Conclusion

In conclusion, I believe that I have made significant progress on the goals outlined in my Era of Hope Scholar Research Award.

Tumor-associated macrophages and stromal TNF-α play central roles in the regulation of collagen structure in breast tumor models as visualized by second harmonic generation.

Burke, Ryan M.[1]; Madden, Kelley S.[1]; Perry, Seth W.[1]; Zettel, Martha L.[2]; Brown, Edward B. III[1,*].

1. Department of Biomedical Engineering, University of Rochester: Box 639, 601 Elmwood Avenue, Rochester, NY 14627.
2. Department of Neurobiology and Anatomy, University of Rochester Medical Center. 575 Elmwood Avenue, Rochester, NY 14642.

*Corresponding author

Email addresses:

1. ryan_burke@urmc.rochester.edu
2. kelley_madden@urmc.rochester.edu
3. seth_perry@urmc.rochester.edu
4. martha_zettel@urmc.rochester.edu
5. edward_brown@urmc.rochester.edu

Abstract

Introduction: Collagen I fibers that are visible with second harmonic generation (SHG) are associated with efficient tumor cell locomotion, and preferential locomotion along these fibers correlates with a more aggressively metastatic phenotype. Through mechanisms that are not yet well understood, macrophages are able to manipulate the structure of collagen fibers in the developing murine breast with SHG as a readout of collagen fiber structure, without affecting the total amount of collagen present as quantified by immunofluorescence (IF). Tumor-associated macrophage (TAM) infiltration in breast tumors correlates with poor prognosis and increased likelihood of metastasis in the clinic, making TAMs an interesting and accessible therapeutic target. Furthermore, TAMs are known to produce tumor necrosis factor alpha (TNF-α), which has differential effects on breast cancer cells and stromal fibroblasts, and treatments known to affect macrophage cytokine production have likewise been shown to affect tumor SHG. Taken together, these facts suggest TAMs and stromal expression of TNF-α may play a role in collagen organization in the tumor. ***Methods:*** We compared SHG and IF signals from tumors grown in mice with and without TNF-α, in the presence or absence of TAMs. Results were compared with t-tests and ANOVA as appropriate. ***Results:*** Using liposome-encapsulated clodronate to specifically deplete TAMs, we show for the first time that modulation of TAM presence alters tumor collagen fibrillar structure on a molecular level as quantified by SHG and IF. This alteration in structure correlates with a decrease in lung metastases. Furthermore, we show that abrogation of TNF-α expression by tumor stromal cells also alters fibrillar structure, and that subsequent modulation of TAM presence has no effect on these signals. In each case, metastatic burden again correlates with optical readouts of collagen structure. ***Conclusions:*** Our results implicate TAMs and stromal TNF-α as a regulator of collagen structure in the metastatic breast tumor, and suggest that this structure may in

turn play a role in tumor metastasis. These findings represent a novel mechanistic role by which TAMs exert tumor- and- metastasis-promoting effects *in vivo* to complement and amplify their already-characterized immunological functions.

Keywords

Breast cancer, collagen type I, second harmonic generation, immunofluorescence, tumor-associated macrophage, tumor necrosis factor alpha, multiphoton microscopy, metastasis.

Introduction

SHG is defined as the nonabsorptive combination of two excitation photons into one emission photon of exactly half the wavelength and twice the energy of the individual incoming photons[1, 2]. SHG is a coherent phenomenon (the scatterers produce emission waves exhibiting a constant phase relationship), and as such is dependent on the ordering of the individual scatterers [3]. For example, scatterers oriented in regular rows in parallel can produce significant constructive and destructive interference in certain directions, while a randomly positioned assortment of scatterers would produce minimal net constructive or destructive interference. In the tumor, SHG is produced primarily by fibrillar collagen and the scatterers are the individual collagen triple helices. These helices are bundled together end-to-end and side-by-side into fibrils, which are in turn bundled into generally regularly spaced arrays producing the collagen fiber. As a result of the coherent nature of SHG emission, the SHG detected from a given fiber is influenced by the amount of collagen triple helices in the focal volume as well as the diameter of the fibrils, their spacing, and the degree of order versus disorder in their packing [2, 4, 5].

Collagen I fibers that produce significant detectable SHG have been noted in breast tumor models as pathways of improved tumor cell locomotion [6, 7]. This efficient, biased movement along SHG-producing fibers contrasts strongly with the random walk exhibited by cells moving independently of the fibers, and also positively correlates with increased metastatic behavior [8, 9]. This prometastatic role is enhanced by a tendency of SHG-producing fibers to orient themselves radially within tumors, extending outward to and through the tumor-host interface [8]. The areas where these fibers cross the interface has been shown to be associated with tumor cells intravasating into healthy tissue, one step in metastasis to distant organs [8]. Based upon these observations, as well as the demonstration that therapeutic alteration of the tumor collagenous matrix (as quantified with SHG) led to an alteration in

drug transport within the tumor, we hope to dissect the cells and signals responsible for the manipulation of collagen fiber structure, using SHG as a readout [3]. This may in turn lead to novel therapeutic targets to manipulate the matrix and hence alter metastatic output and/or drug delivery.

To distinguish changes in fiber structure from altered collagen concentration (which are both of interest), we will compare SHG emission signal to signal from collagen I immunofluorescence. The SHG signal from a given focal point in a multiphoton laser-scanning microscope is sensitive to collagen fiber structure, including fibril diameter, spacing, and internal order versus disorder, as well as collagen content in the focal volume, while IF relies on epitope recognition and therefore yields information as to the total number of accessible epitopes present in the focal volume. We will therefore define the ratio of SHG to IF as an "ordering index", or OI. Changes in the OI can then be interpreted as changes primarily in collagen fiber structure, distinct from the total collagen content, and the OI can be determined readily on a pixel-by-pixel basis using simultaneous image capture in two color channels (Supplemental Figure 1). We can then observe systemic changes in collagen I structure by calculating the average OI over entire images taken in animals that have undergone a response to putative structure-modulating stimuli. These changes may be occurring throughout the tumor stroma (globally) or in localized areas of interest surrounding features implicated in metastasis such as blood vessels or the tumor/host interface. Note that changes in OI of a pixel from a given fiber indicate local changes in the microscopic structure of that fiber, perhaps due to alterations in fibril diameter, spacing, or order vs. disorder *within the fiber*. But they do not indicate changes in macroscopic fiber orientation (for example with respect to the tumor/host interface), its alignment with other distant fibers outside the focal volume, or other macroscopic structural changes.

Breast tumors are not composed solely of tumor cells, but also host cell types including hematopoietic and stromal cells of which up to approximately 50% may be macrophages [10, 11].

Leukocyte infiltration in the breast tumor, originally thought to simply indicate an anti-tumor response, has been recognized as far more complicated. While T cell infiltration and the presence of M1-polarized (classically activated) macrophages indicate anti-tumor activity, M2-polarized (alternatively activated) macrophage infiltration is now recognized as a crucial factor in promotion of tumor growth and spread by production of signals beneficial to the tumor cells' survival and proliferation [10, 12]. Clinical data indicate that high densities of leukocyte infiltration, particularly M2-polarized macrophage invasion, correlate with poor clinical prognosis and increased instance of metastatic disease [13, 14]. M2-polarized macrophages play a role in resolution of inflammation via high endocytic clearance and synthesis of growth factors, as well as reduced pro-inflammatory cytokine secretion. TAMs are uniquely suited to tumorigenic promotion – they produce a wide variety of growth factors, cytokines, matrix-altering enzymes, and chemokines that coordinate to assist in matrix remodeling and improved angiogenesis, both requirements for successful tumor growth [10]. Hence we have identified the TAM as a promising candidate for a cell that manipulates collagen structure.

The identification of the TAM as a candidate cell that manipulates collagen structure is supported by one key recent study, in which mice deficient in colony stimulating factor one (CSF-1, a protein essential to macrophage proliferation, survival, and chemotactic recruitment) showed marked alterations in terminal end bud formation in the mammary duct [15]. Abortive development of the end bud was noted, as well as a steep decrease in the SHG in focal volumes around the mammary duct. Curiously enough, the total amount of collagen present as detected by IF was unaffected. This represents a decrease in OI accompanying the loss of macrophages in the breast bud area represents and identifies macrophages as a cell type capable of affecting OI. A previous study showed that upon treatment with the hormone relaxin, soft tissue sarcomas respond by altering collagen I structure with SHG intensity as a readout[3]. Relaxin binds specifically to macrophage glucocorticoid receptors, which results in alterations in macrophage cytokine expression panels [16]. The binding of relaxin to

glucocorticoid receptors results in negative modulation of TNF-α expression by macrophages *in vitro* [17]. Hence we have identified TAMs as candidate cells, and TNF-α signaling as a candidate signaling molecule to manipulate the OI.

Evidence for TNF-α signaling affecting collagen and the cells that are able to produce and organize it is widespread. On a genetic level, TNF-α is able to induce COX-2 promoter activation via upregulation of p300 binding and p50 acetylation in human foreskin fibroblasts, which is an important step in inflammation, angiogenesis, and tumor promotion [18-20]. Interestingly, TNF-α is also shown by recent *in vivo* literature to be essential to primary growth and metastatic progression in Lewis lung carcinoma [21].

We therefore hypothesize that TAMs can affect collagen fiber structure in tumors, as measured by the OI, and that this is accomplished through TAM expression of TNF-α. To test this hypothesis, we grew a breast tumor cell line (E0771, a mammary adenocarcinoma derived from C57Bl/6 mice) in both wildtype mice and mice incapable of expressing TNF-α. Additionally, in both types of mice TAM presence was modulated by periodic injections of clodronate-containing liposomes (ClodL)[22]. OI and metastatic burden were evaluated, and we show for the first time that expression of TNF-α by the host stromal cells of the tumor affect collagen structure (as measured by OI), that TAMs affect collagen structure in tumors, and that the influence of TAMs and stromal TNF-α expression is not additive. We also show that these effects on collagen structure each correlate with a significant decrease in metastatic events, and hence that these results may provide a platform for therapies that manipulate collagen structure and thereby impact the metastatic output of the tumor.

Materials and Methods

Cells and Reagents

A murine medullary mammary adenocarcinoma syngeneic with C57Bl/6 mice (E0771, Roswell Park Cancer Institute, Buffalo, NY) was maintained in RPMI 1640 medium (Gibco/Invitrogen, Carlsbad, CA) supplemented with 10% gamma-irradiated fetal calf serum (HyClone/Thermo-Fisher, Waltham, MA) and Primocin (InvivoGen, San Diego, CA). Cells were passaged no more than five times before being replaced with frozen stocks. Upon harvest with .25% trypsin/EDTA, cells were centrifuged and resuspended in sterile PBS pending implantation. T47D and MCF-7 human breast cancer cell lines (American Type Culture Collection, Manassas, VA) were also cultured in RPMI 1640 medium for comparative use in *in vitro* proliferation assays. RAW264.7 transformed murine macrophages (ATCC) were used as a positive control for TNF-α production and were cultured in DMEM supplemented with 4.5 g/L glucose, 10% FCS, and Primocin. All lines were tested for mycoplasma contamination bi-monthly using MycoFluor detection kit (Invitrogen, Carlsbad, CA) and only certified mycoplasma-free cultures were used for implantation.

Magnetic Separation

E0771 tumors grown in mammary fat pads were finely minced, washed with RPMI 1640, then shaken in medium supplemented with 0.5 mg/ml of collagenase type D (Sigma-Aldrich, St. Louis, MO) at 37°C for 180 minutes. The cell dispersion was passed through metal mesh (100-µm window) and centrifuged three times with RPMI 1640 at 200x*g* for 10 minutes each. Cells were then labeled with anti-CD11b antibody conjugated to magnetic beads (Miltenyi Biotec, Auburn, CA). To harvest $CD11b^+$ cells, suspensions were applied to a type LS positive selection column with MidiMACS (Miltenyi Biotec) according to manufacturer instructions. Selected cells were cultured to approximately 70% confluence in DMEM supplemented with 10% FCS and Primocin.

Animals and Husbandry

C57Bl/6 female mice (Jackson Laboratories, Bar Harbor, ME) were used between 15 and 19 weeks of age. Mice were housed in standard two-way static (non-ventilated) conditions in groups of five, and were allowed *ad libitum* access to standard food and water. To determine the effects of global deletion of TNF-α , female B6.129S-*Tnf*^{tm1Gkl}/J (Jackson Labs) mice were used between 15-19 weeks of age, and housed as above. C57Bl/6 animals represent a valid control genotype for this knockout. All animal work was done in accordance with University Committee for Animal Resources regulations.

Tumor Implantation and Liposome Administration

Animals were anesthetized with a ketamine/xylazine mixture (90/9 mg/kg body weight) delivered intraperitoneally. The ventral surface of the animal was depilated and $1x10^5$ E0771 cells were implanted in the right inguinal mammary fat pad using a 27-gauge needle. Four hours following this procedure, mice were administered a dose of either PBS- or clodronate-containing liposomes (Encapsula NanoSciences, Nashville, TN) from 5 mg/mL stock solution via the intraperitoneal route using a 27-gauge needle to a concentration of 2 mg/20 g body weight on Day 0 [22]. This intraperitoneal injection was performed every third day at 1 mg/ 20 g body weight. A measure of the long and short axis of each tumor was made during this time with digital calipers, with tumor volume being calculated using the formula for a prolate spheroid ($V = (4/3)\pi N^2 L.$). This was determined to best approximate the shape of the average E0771 tumor, as it has been observed to grow preferentially along the injection track. On Day 27 post-implantation, animals were sacrificed by intraperitoneal injection of sodium pentothial and subsequent cervical dislocation. Half the tumor was snap-frozen in dry ice pending sectioning and immunohistochemistry. The other half was placed in cell culture media pending flow cytometric analysis. Lungs were placed in 10% neutral-buffered formalin for H&E staining.

Flow Cytometry

Tumor halves were finely minced, washed with RPMI 1640, strained through a 70 μm mesh filter to remove debris and centrifuged two times. 2 mL RPMI 1640 was added and the cells were vortexed. 200 μL of this suspension was removed and added to 1 mL RPMI 1640. Cells ($2x10^6$) were incubated at 4°C for 15 minutes in ACK buffer to lyse red blood cells, centrifuged to remove ACK buffer, and resuspended in flow wash buffer consisting of 1% BSA and .25% sodium azide in sterile PBS. Cells were blocked using anti-mouse CD16/CD32 antibody (BD Pharmingen, Franklin Lakes, NJ), then were resuspended in buffer containing either: 1) autofluorescence - buffer only; 2) isotype controls – 1:50 peridinin chlorophyll-conjugated rat IgG_{2a} (BD Pharmingen, Franklin Lakes, NJ), or 3) experimental samples - a 1:50 dilution of FITC-conjugated rat (IgG_{2a}) anti-mouse F4/80 (Abcam, Cambridge, MA). Cells were incubated in the dark for 30 minutes at 4°C. Cells were then centrifuged and resuspended in flow wash buffer twice. Cells were stored in 4% paraformaldehyde in the dark pending flow sorting using a FACSAria flow cytometer (BD Biosciences, Franklin Lakes, NJ) equipped with FlowDiVa software.

ELISAs and Sample Preparation

A Quantikine enzyme-linked immunosorbent assay (ELISA) kit specific to mouse TNF-α (R&D Systems, Minneapolis. MN) with a sensitivity of 5.1 pg/mL was employed to measure TNF-α in cell culture supernatants and tumor lysates. To prepare cell culture supernatants, cells were grown to 70% confluence in a T-75 tissue culture flask, then media was removed and replaced with reduced serum media for 48 hours. This media was removed, centrifuged, and immediately assayed following the manufacturer's instructions. Tumor lysates were prepared by homogenization of excised tumor tissue in RIPA buffer containing sodium deoxycholate and HALT protease/phosphatase inhibitor (Pierce Protein Research, Rockford, IL). Lysates were then centrifuged at 18,000x*g* for 10 minutes and assayed per manufacturer's instructions. To determine total protein concentration in these lysates for standardization purposes, a bicinchoninic acid (BCA) assay was employed (Pierce Protein Research) in which samples were diluted 1:20 in RIPA buffer in 96-well plates, then incubated with the working

reagents for 2 hours and compared to standards prepared per manufacturer specifications. To determine TNF-α levels, a plate reader (BioTek, Burlington, VT) equipped with Gen5 software measuring absorbance at 450 and 570 nm was used to generate standard curves and sample concentrations. To determine total protein levels, absorbance at 562 nm was measured.

Proliferation Assays

In vitro proliferation was determined with the use of a CyQuant Cell Proliferation Assay (Molecular Probes/Invitrogen, Carlsbad, CA) following manufacturer's instructions. Specifically, a plate reader (BioTek) exciting bound dye at 480 nm and detecting at 520 nm was used to generate values for nuclear (DNA) fluorescence in octuplicate.

Immunohistochemistry

Snap-frozen tumor halves were sectioned at 7 μm on a cryostat (Reichert-Jung, Depew, NY) at -21°C and static-mounted on positively charged slides (VWR). Sections were mounted such that each slide contained at least four sections from each of the four genotype/therapy groups in an attempt to minimize possible staining artifacts between samples. Sections were fixed in a 3:1 mixture of acetone/methanol for 20 minutes at -20°C. Slides were rehydrated twice in sterile PBS for 5 minutes, then placed in peroxidase blocking solution (5% BSA, .2% Triton-X100) for one hour, followed by two 5 minute PBS washes. Sections were incubated at room temperature in a humidified chamber with a solution of PBS containing .5% BSA and combinations of the following antibodies: 1) rabbit anti-mouse collagen I (Abcam, Cambridge, MA), 1:200 dilution; 2) FITC-conjugated rat IgG_{2a} anti-mouse CD31 (BD Pharmingen, Franklin Lakes, NJ), 1:500 dilution); or 3) FITC-conjugated rat IgG_{2a} anti-mouse F4/80, 1:50 dilution. To detect rabbit anti-mouse collagen I, sections were then washed as before and incubated for two hours in AlexaFluor 594-conjugated goat anti-rabbit IgG (Invitrogen, Carlsbad, CA), 1:500 dilution. To assure optimal binding to all accessible epitopes, serial dilutions of collagen I antibody were

accomplished to determine optimal concentration for antibody binding and peak fluorescence. Slides were then washed and coverslipped in Prolong Gold AntiFade without DAPI (Invitrogen, Carlsbad, CA) and allowed to dry 24 hours before imaging. Automated H&E staining (Dako, Carpinteria, CA) was performed on 3 μm rotary microtome sections of paraffin-embedded lungs.

Evaluation of Metastatic Burden

H&E-stained lung sections were obtained at every 50 μm through the lung and evaluated by a blinded observer using a light microscope (Olympus BX-51, Center Valley, PA) set to brightfield. Metastatic cells were identified by several criteria: high ratio of hematoxylin relative to eosin, surrounding abnormalities in lung structure, abnormal shape/size of nuclei and/or presence of abnormal mitotic spindles, and differences in cell shape and size. Presence of a single cell was quantified as a metastatic event, and results are presented as averages of metastatic number in ten sections of lung per animal.

Imaging and Image Analysis

Slides were imaged by a blinded observer using a custom-built two-photon microscope (Olympus). Two-photon excitation was provided by a MaiTai Ti:sapphire laser providing 100 fs pulses at 80 MHz and 810 nm. Beam scanning and image acquisition were performed with a Fluoview FV300 scanning system interfaced with a BX61WI upright microscope (Olympus, Center Valley, PA). The focusing objective is a UMPLFL20XW water immersion lens (20×, 0.5 N.A., Olympus, Center Valley, PA). The objective was used to focus the excitation beam on the sample and at the same time collect both backscattered SHG signal and the two-photon excitation fluorescence from the antibodies of interest. The backscattered SHG signal and two-photon fluorescence were separated from the excitation beam by a dichroic mirror (670 DCSX, Chroma, Rockingham, VT) and the resultant beam was passed through another dichroic mirror to differentiate into separate channels of SHG and two-photon fluorescence

(475 DCSX, Chroma, Rockingham, VT). SHG was collected with a band pass filter centered at 405 nm (HQ405/30m-2P, Chroma, Rockingham, VT) and detected by a photomultiplier tube (HC125-02 Hamamatsu Corporation, Hamamatsu, Japan). The two-photon excitation fluorescence signal was collected with either a band pass filter centered at 530 nm (HQ530/30m-2P, Chroma, Rockingham, VT) or a bandpass filter centered at 635 nm (HQ635/30m-2P, Chroma, Rockingham, VT). For the 635 nm filter case, the PMT used is more red-sensitive (Hamamatsu HC125-01) and the emission signal passed through two filters before being detected by the second PMT, the second filter being a short pass filter (Chroma E700SP-2P) that is used to block residual effects from the 810 nm excitation beam. Resulting images are 680 microns across. Laser power was monitored and kept constant throughout the experiment and across experimental repetitions, as was the voltage across PMTs.

Image analysis was performed as follows. In ImageJ (Rasband, W.S., ImageJ, U. S. National Institutes of Health, Bethesda, Maryland, USA, http://imagej.nih.gov/ij/, 1997-2011), the background was defined by the average pixel counts of an image with no excitation laser, and subtracted from the raw SHG and IF images. Then each image was thresholded by a blinded observer to set collagen fiber pixels to 1 and any remaining dim background pixels to zero, producing an "SHG mask" and an "IF mask". The SHG image was multiplied by the SHG mask, producing the "masked SHG image", and the IF image was multiplied by the IF mask to produce the "masked IF image". The average pixel count of the masked SHG image, divided by the average pixel count of the SHG mask, is then the average pixel count of those pixels above threshold, i.e. within collagen fibers. Likewise with the masked IF image. The average SHG pixel count, IF pixel count, and their ratio, of those pixels within collagen fibers is then reported as the images' SHG, IF, and OI, respectively.

Statistical Analysis

Statistical analysis was performed using Prism 5 software (GraphPad, La Jolla, CA). Student's (unpaired) t-tests were employed to make pairwise comparisons where appropriate. For multiple groups, if a

significant main effect was found, one-way ANOVA was used with Bonferroni post-tests to adjust for multiple comparisons. To analyze differential effects of macrophage depletion and TNF-α absence on SHG, IF, and OI, two-way ANOVA was used with Bonferroni post-tests to adjust for multiple comparisons. Growth curves for tumors were assessed by one-way ANOVA with repeated measures, with Bonferroni post-hoc analysis. Probability values (p) less than or equal to .05 were considered significant differences between groups.

Results

E0771 does not produce significant TNF-α nor proliferate in response to it in culture or in animal models

Pilot experimentation was required to determine the answers to two key issues: 1) the presence or absence (and importance) of autocrine TNF-α production by the E0771 tumor, and 2) the response of E0771 to TNF-α in the microenvironment. To determine the levels of TNF-α produced by E0771 cells in culture, a sandwich ELISA kit was employed to assay cell culture supernatants. E0771 cells at 75% confluence did not produce measurable TNF-α (less than 5.1 pg/mL) in culture (Figure 1). To activate RAW264.7 cells, lipopolysaccharide (LPS, E. coli serotype 026:B6, Sigma-Aldrich, St. Louis, MO) was added to media at 100 ng/mL for 24 hours prior to assaying for TNF-α. RAW 264.7 macrophages were assayed in both normal and LPS-activated conditions, and showed significant levels of TNF-α production in culture, suggesting that any detectable TNF-α production in the tumor environment is likely to originate in the host cells, and specifically in macrophages (which may account for up to half of the mass of the solid tumor) [11]. To confirm this, macrophages isolated from E0771 tumors using magnetic antibody separation targeted to CD11b (a myeloid marker) showed the ability to produce TNF-α at significant levels in culture. To further examine this, E0771 tumors were grown in both wildtype and TNF-$\alpha^{(-/-)}$ animals. TNF-α was present in significantly higher quantities in wildtype-derived tumors

as opposed to those tumors grown in TNF-$\alpha^{(-/-)}$ mice, where levels were again undetectable (below 5.1 pg/mL, Figure 2). Taken together, these results suggest that the E0771 cell line is not a source of TNF-α production *in vitro* or *in vivo*, and that E0771-associated macrophages, as expected, are a primary source of this signal *in vivo*.

After eliminating tumor cell TNF-α production from E0771 as a possible source of signaling, the proliferative response of E0771 to TNF-α was determined using a fluorescent DNA-binding dye kit (CyQuant). This was prompted by the fact that in a different mouse model of breast cancer (T47D), TNF-α was shown to directly promote mitogenic signaling by binding to TNFR1 and activating p42/p44 MAPK, JNK, PI3-K/Akt pathways and NF-κB transcriptional activation [23]. Furthermore, in that model, application of TNF-α supported tumor growth, and selective small molecule inhibition of NF-κB activity resulted in tumor regression. Conversely, TNF-α induced apoptosis in MCF-7 breast cancer cells *in vitro* [24]. To determine the response of E0771 cells to TNF-α, we incubated cells for 48 hours in either control media or media containing 20 ng/mL TNF-α (Figure 3). TNF-α did not significantly alter proliferation of E0771, in direct contrast to the human breast tumor cell line T47D, which showed a marked increase in proliferation in response to 20 ng/mL TNF-α, as found in the literature [23]. Furthermore, MCF-7 cells exposed to this level of TNF-α exhibited significant reduction in proliferation, also as found in the literature [24]. Therefore, TNF-α does not significantly stimulate E0771 proliferation nor significantly inhibit its growth.

Evaluation of ClodL on E0771 Proliferation In Vitro

To determine whether clodronate liposome (ClodL) therapies directly alter E0771 cell or stromal fibroblast viability, we compared the effects of ClodL therapy on these cell types *in vitro*. ClodL therapy markedly inhibited the survival of the RAW264.7 transformed murine macrophage cell line in a dose-

dependent manner, while having no effect relative to PBSL therapy in HFF-1 human foreskin fibroblasts nor E0771 breast cancer cells at equivalent concentrations as determined by CyQuant assay (Figure 4).

Evaluation of ClodL on TAM Depletion In Vivo

TAM depletion efficiency as quantified by flow cytometry using FITC-conjugated antibody against F4/80 indicates that mice exposed to ClodL experience 97.5 ± 6.4 % depletion of $F4/80^{+}$ cells in the wildtype cohort and 96.4 ± 11.7 % depletion in the TNF-$\alpha^{-/-}$ cohort (Figure 5).

Effects of TAM Depletion and TNF-a Abrogation on SHG

TAM depletion and TNF-α knockout both alter the intensity of SHG-producing fibers in the E0771 tumor (Figure 6a). Two-way analysis of variance shows a strong main effect of TAM depletion ($p<.0001$) with no main effect resulting from TNF-α knockout ($p=.3122$). However, the variables strongly interact ($p=.0004$), making further analysis necessary. A one-way analysis of variance indicates a main effect of treatment on SHG ($p<.0001$), and Bonferroni post-hoc analysis shows that wildtype/PBSL mice show significantly ($p<.05$) elevated SHG relative to all other groups. TNF-$\alpha^{(-/-)}$/PBSL mice also show elevated SHG relative to wildtype/ClodL mice ($p<.05$), but not relative to TNF-$\alpha^{(-/-)}$/ClodL mice. Both groups of ClodL-treated mice exhibit statistically equivalent levels of SHG ($p>.05$). From these analyses, we can determine that growth in the presence of TAM depletion results in a significant decrease in SHG in E0771 tumors, as does growth during attenuation of stromal TNF-α, but to a lesser extent. Furthermore, in the absence of TAMs, depletion of TNF-α has no further effect on SHG while in the absence of TNF-α, depletion of TAMs has no further effect

Effects of TAM Depletion and TNF-a Abrogation on IF

SHG is dependent upon collagen content as well as fiber structure. Therefore, in order to normalize the SHG intensity to the total amount of collagen I present, we must first quantify collagen content with IF. TAM depletion and stromal TNF-α knockout both alter detected collagen I fiber IF in the E0771 tumor (Figure 6b). Two-way analysis of variance shows a strong main effect of both TAM depletion and TNF-α knockout (both $p<.0001$). The variables again show a significant degree of interaction ($p=.04$), making further analysis necessary. A one-way analysis of variance indicates a main effect of treatment on IF ($p<.0001$), and Bonferroni post-hoc analysis shows that wildtype/PBSL mice show significantly reduced IF values compared to all three remaining groups ($p<.05$). Furthermore, though IF signal in tumors grown in wildtype/ClodL mice is statistically equivalent to that of both TNF-α knockout groups ($p>.05$), tumors grown in TNF-$\alpha^{(-/-)}$/PBSL mice exhibit less IF than do tumors grown in TNF-$\alpha^{(-/-)}$/ClodL mice ($p<.05$). We therefore conclude that growth in the presence of TAM depletion results in a significant increase in IF in E0771 tumors, as does growth during attenuation of stromal TNF-α, to the same extent. Furthermore, in the absence of TAMs, depletion of stromal TNF-α has no further effect on IF. However, in the absence of stromal TNF-α, depletion of TAMs further increases IF.

Effects of TAM Depletion and TNF-a Abrogation on OI

Division of the SHG signal by the IF signal produces the order index (OI), which is primarily sensitive to changes in fibrillar structure, such as fibril diameter, spacing, and order vs disorder in fibrillar packing [1-5]. Two-way analysis of variance shows a strong main effect of both TAM depletion and stromal TNF-α knockout ($p<.0001$ and $p=.013$ respectively) on OI (Figure 6c). The variables again show a significant degree of interaction ($p=.0027$), making further analysis necessary. A one-way analysis of variance indicates a main effect of treatment upon OI ($p<.0001$), and Bonferroni post-hoc analysis shows that wildtype/PBSL mice have significantly elevated OI relative to the three remaining groups ($p<.05$). However, none of the three remaining groups exhibit significant differences between their mean OI values ($p>.05$).

Metastatic burden correlates negatively with both TAM presence and TNF-α expression

To ascertain a possible relationship between modulations in OI and modulations in metastatic burden, lungs were resected, sectioned, and stained with hematoxylin and eosin, then imaged to determine the extent of metastasis (Figure 7 and Supplemental Figure 2). E0771 readily metastasizes to the lung from the primary site, and therefore makes an excellent candidate for such studies [25]. Two-way analysis of variance shows a strong main effect of both TAM depletion and lack of TNF-α on metastatic burden ($p=.0006$ and $p<.0001$ respectively. The degree of interaction is again significant ($p=.0007$), making further analysis necessary. A one-way analysis of variance indicates a main effect of treatment upon the incidence of metastasis ($p<.0001$) and Bonferroni post-hoc analysis shows that while wildtype/PBSL mice exhibit significantly ($p<.05$) higher metastatic burden than any of the other groups, the other three groups do not show distinguishably different metastatic burdens ($p>.05$). We conclude that both TAM depletion and TNF-α knockout result in significant decreases in metastatic events, and that these decreases correlate well with OI values in the E0771 tumor.

Evaluation of ClodL on E0771 Proliferation In Vivo

To determine whether E0771 tumors *in vivo* show alterations in multiplicity (volume standardized to volume at Day 3 post-injection) in response to the presence or absence of TNF-α and/or macrophages, tumors implanted in either C57Bl/6 wildtype or TNF-$\alpha^{(-/-)}$ mice and exposed to PBS or ClodL treatment were measured over the course of 27 days of tumor growth (Figure 8). Wildtype mice exposed to PBSL therapy bore significantly larger tumors ($p<.05$) at 27 days compared to any other group ($p<.05$) while the other three groups did not show distinguishably different tumor sizes ($p>.05$).

Discussion

In this set of studies we elucidated a novel mechanistic role for tumor associated macrophages and stromal cell expression of TNF-α in the evolution of collagen structure during tumor growth and an influence this may have on metastasis, in a murine model of breast cancer. In doing so, we made use of the E0771 murine mammary adenocarcinoma, a metastatic cell line syngeneic with the C57Bl/6 mouse. The choice of this cell line was predicated on the availability of the knockout strain B6.129S-*Tnf*^{tm1Gkl}/J, which is incapable of expressing TNF-α. We first established that the E0771 tumor model does not produce TNF-α, is nonresponsive to TNF-α, and that it also does not have an intrinsic cellular response to liposome-encapsulated clodronate therapies that target TAMs. Next, we established that these therapies are able to alter the structure of collagen I fibers (as measured by the OI) and metastatic burden.

Taken together, our OI data suggest that in the E0771 model of metastatic breast cancer, TAMs influence collagen structure (Fig. 6c, columns 1 and 2 are different), and that stromal TNF-α influences collagen structure (Fig. 6c, columns 1 and 3 are different). This suggests three main models: A) TAMs and TNF-α influence OI independently, B) TNF-α influences OI via its action on TAMs, and C) TAMs influence OI via expression of TNF-α. Model A is unlikely because in the absence of TAMs modulation of TNF-α has no further effect on OI (Fig. 6c, 2 and 4 are the same) *and* in the absence of TNF-α modulation of TAMs has no further effect on OI (Fig. 6c, 3 and 4 are the same). However, Models B and C are consistent with our observations, and can be further refined. If TNF-α influences OI via action on TAMs (Model B), our data further suggests that TNF-α acts *only* via TAMs because in the absence of TAMs modulation of TNF-α has no further effect on OI (Fig. 6c, 2 and 4 are the same). Furthermore, in that model our data also suggests that *no other* molecule is constructively stimulating TAMs to influence OI because in the absence of TNF-α modulation of TAMs has no further effect on OI (Fig. 6c, 3 and 4 are the same). Lastly, if TAMs influence OI via their expression of TNF-α (Model C), our data suggests that

TAMs influence collagen structure primarily through their TNF-α expression and not via other mechanisms because in the absence of TNF-α modulation of TAMs has no further effect on OI (Fig. 6c, 3 and 4 are the same). Furthermore, in that model our data also suggests that there are no other significant host cell types utilizing TNF-α to influence collagen structure because in the absence of TAMs modulation of TNF-α has no further effect on OI (Fig. 6c, 2 and 4 are the same). Ongoing studies are aimed at determining whether these interpretations hold up in similar experimental model systems.

In addition to these primary observations, there are two secondary observations: TAM presence was able to modulate IF in the absence of stromal TNF-α (Fig. 6b, 3 and 4 are different) and attenuation of TAM presence produced a greater SHG reduction than attenuation of stromal TNF-α (Fig. 6a, 2 and 3 are different). In Model B (TNF-α operates via TAMs) these two observations imply that there may be other less significant mechanisms, in parallel with TNF-α, which induce TAMs to influence collagen structure. In Model C (TAMs operate via TNF-α), these two observations imply that there may be other less significant mechanisms by which TAMs affect tumor collagen in addition to their expression of TNF-α. However, note that the observation that attenuation of TAM presence produced a greater SHG reduction than the attenuation of stromal TNF-α is based upon quantitative comparison of the results of two very different experimental manipulations (TAM depletion vs TNF-α knockout) and may simply be a result of different efficiencies in the two methods.

Note that when macrophage recruitment is specifically disabled in developing mouse mammary tissue, the structure of collagen fibers but not their total amount, as measured by SHG and IF, is altered with negative consequence to normal maturation [15]. Interestingly, in contrast to our observations, this study noted a similar decrease in SHG, but without any elevation in IF. This may be due to myriad structural differences between normal and diseased mammary fat pad – in particular, the well-documented ability of cancer cells to produce stimuli inducing fibroblasts to transition to a more active

myofibroblast phenotype, with one consequence being elevated levels of collagen production[26]. Additionally, this may simply be due to differences in antibody-epitope binding between two different model systems.

Our observations that TAMs and stromal TNF-α play a role in altering tumor collagen structure as quantified by the OI are consistent with established roles for both in modulating tumor stroma. Autocrine TNF-α signaling has been noted as necessary to induce high levels of expression of monocyte MMP-9, a gelatinase that is active on basement membrane, via the transcription factor Egr-1[27-30]. TNF-α has also been shown to sharply increase MMP-14 levels in concert with CCL4, a C-C chemokine, in a monocytic human cell line [31]. MMP-14 is able to subsequently activate MMP-2, another gelatinase capable of degrading basement membrane. However, note that the nonfibrillar collagens in basement membrane do not generate SHG and were not studied here. Importantly, both direct application of TNF-α and indirect production of it through LPS stimulation of macrophages have been shown to upregulate MMP-1a, -1b, -3, and -13 in rat synovia, and these MMPs can directly affect the fibrillar collagen responsible for SHG signal [32].

Our demonstration of a novel role for TAMs and TNF-α in manipulating collagen structure in the tumor extracellular matrix naturally leads us to ask: what are the possible consequences of this manipulation? As discussed above, there is ample evidence in the literature that collagen structure, as quantified with SHG, influences tumor metastasis, including evidence that efficient tumor cell locomotion through the tumor is favored by the presence of SHG-producing fibers, and that this locomotion along SHG+ fibers correlates with metastatic output [1, 7-9]. Consistent with this, our data demonstrates that alterations in collagen structure as quantified by the OI correlated with alterations in metastatic output (Figs. 6c and 7), for in each case wildtype mice treated with PBSL had significantly

greater OI and metastatic output than all other treatment groups, and all other treatment groups were not statistically significantly different from each other.

The link between TAMs, stromal TNF-α, and metastatic output in this tumor model is consistent with recent observations that myeloid cells, of which TAMs are an exemplar, have specifically been implicated as a necessity for the formation of Lewis lung carcinoma metastasis, and their expression of TNF-α was shown to be essential to establishment and growth of the primary tumor and its subsequent metastasis[21]. However, while our observations establishes an interesting link between TAMs, stromal TNF-α, and metastatic output in this tumor model, it does not prove that the metastatic effects are transduced via collagen fiber structure itself, and it may be other effects of TAMs and stromal TNF-α expression that assist in the induction of alterations in metastatic output. For example, our data also demonstrates that tumor growth is correlated with OI, and in turn with metastatic burden (Figs. 6c, 7, and 8). Hence TAMs and stromal TNF-α may instead influence tumor growth via alterations in collagen matrix structure (note that TNF-α does not directly affect E0771 proliferation *in vitro*), and the altered metastatic output may be a result of the different tumor burden. Or all three effects (OI, tumor growth, and metastatic output) may share a common cause but operate via independent mechanisms (for example TNF-α has also been shown to increase migration in human chondrosarcoma cells *in vitro* by upregulating αvβ3 integrin expression through the activation of the MEK/ERK/NF-κB signaling pathway [33]).

Conclusions

In summary, we show for the first time that TAMs as well as stromal TNF-α expression are responsible for significant alterations in the structure of collagen I fibers within the metastatic breast tumor (as indicated by the OI). We further demonstrate that this effect is implemented either via TAM

expression of TNF-α or stromal TNF-α action on TAMs, and that parallel pathways via other cell types or other cytokines are considerably less significant. Lastly, we show that the effects of TAMs and stromal TNF-α on tumor collagen structure is correlated with effects on metastatic output, consistent with previous literature connecting SHG and metastatic output, but that a causal connection is not proven.

Discovering a key role for tumor-associated macrophages and stromal TNF-α in influencing the structural properties of tumor collagen, as measured by SHG, is interesting because of the previously observed effects of these SHG-producing fibers on metastasis of the primary breast tumor, as well as the previously observed relationship between SHG signal and drug transport in tumors [1, 3, 7-9]. These findings suggest that manipulation of SHG measures of collagen structure may in turn manipulate the transport of drugs through tumor tissue, as well as manipulate metastatic output of tumors.

List of Abbreviations

BSA: bovine serum albumin

COX-2: cyclooxygenase-2 (prostaglandin endoperoxide synthase 2)

CSF-1: colony stimulating factor-1

ELISA: enzyme-linked immunosorbent assay

H&E: hematoxylin and eosin

IF: immunofluorescence

MMP: matrix metalloproteinase

MPLSM: multiphoton laser scanning microscopy

NA: numerical aperture

OI: ordering index

PBS: phosphate-buffered saline

PMT: photomultiplier tube

SHG: second harmonic generation

TAM: tumor-associated macrophage

TNF-α: tumor necrosis factor alpha

Competing Interests

The authors declare that they have no competing interests.

Author Contributions

1. RMB completed all experimentation as seen in the manuscript and wrote the first draft of the manuscript.
2. KSM designed some of the experiments, undertook pilot studies, and performed statistical analysis as well as extensive editing of the manuscript.
3. SWP was centrally involved in data interpretation and critical revision of the manuscript.
4. MLZ designed the immunofluorescence regimen and undertook pilot studies.
5. EBB III conceived of the study and participated in design and coordination as well as extensive editing of the manuscript.

All authors have read and approved of the manuscript as submitted.

Author Information

Acknowledgments

The authors wish to acknowledge Tracy Bubel and Khawarl-Jamma M. Liverpool for their indispensable technical assistance, and Dr. Peter Salzman for his assistance with statistical analysis. This work was funded by Department of Defense Breast Cancer Research Program (BCRP) Era of Hope Scholar Research Award W81XWH-09-1-0405 and NIH Director's New Innovator Award 1DP2OD006501 (to EBB), BCRP Idea Award W81XWH-10-01-0087 and NIH R21CA152777-01 (to KSM), and NIH R21DA030256 (to SWP).

•

References

1. Raub CB, Suresh V, Krasieva T, Lyubovitsky J, Mih JD, Putnam AJ, Tromberg BJ, George SC: **Noninvasive assessment of collagen gel microstructure and mechanics using multiphoton microscopy.** *Biophys J* 2007, **92:**2212-2222.
2. Han X, Burke RM, Zettel ML, Tang P, Brown EB: **Second harmonic properties of tumor collagen: determining the structural relationship between reactive stroma and healthy stroma.** *Opt Express* 2008, **16:**1846-1859.
3. Brown E, McKee T, diTomaso E, Pluen A, Seed B, Boucher Y, Jain RK: **Dynamic imaging of collagen and its modulation in tumors in vivo using second-harmonic generation.** *Nat Med* 2003, **9:**796-800.
4. Lacomb R, Nadiarnykh O, Campagnola PJ: **Quantitative second harmonic generation imaging of the diseased state osteogenesis imperfecta: experiment and simulation.** *Biophys J* 2008, **94:**4504-4514.
5. Lacomb R, Nadiarnykh O, Townsend SS, Campagnola PJ: **Phase Matching considerations in Second Harmonic Generation from tissues: Effects on emission directionality, conversion efficiency and observed morphology.** *Opt Commun* 2008, **281:**1823-1832.
6. Wang W, Wyckoff JB, Frohlich VC, Oleynikov Y, Huttelmaier S, Zavadil J, Cermak L, Bottinger EP, Singer RH, White JG, et al: **Single cell behavior in metastatic primary mammary tumors correlated with gene expression patterns revealed by molecular profiling.** *Cancer Res* 2002, **62:**6278-6288.
7. Sidani M, Wyckoff J, Xue C, Segall JE, Condeelis J: **Probing the microenvironment of mammary tumors using multiphoton microscopy.** *J Mammary Gland Biol Neoplasia* 2006, **11:**151-163.
8. Provenzano PP, Eliceiri KW, Campbell JM, Inman DR, White JG, Keely PJ: **Collagen reorganization at the tumor-stromal interface facilitates local invasion.** *BMC Med* 2006, **4:**38.
9. Wyckoff JB, Wang Y, Lin EY, Li JF, Goswami S, Stanley ER, Segall JE, Pollard JW, Condeelis J: **Direct visualization of macrophage-assisted tumor cell intravasation in mammary tumors.** *Cancer Res* 2007, **67:**2649-2656.
10. Pollard JW: **Tumour-educated macrophages promote tumour progression and metastasis.** *Nat Rev Cancer* 2004, **4:**71-78.
11. Direkze NC, Hodivala-Dilke K, Jeffery R, Hunt T, Poulsom R, Oukrif D, Alison MR, Wright NA: **Bone marrow contribution to tumor-associated myofibroblasts and fibroblasts.** *Cancer Res* 2004, **64:**8492-8495.
12. Ochsenbein AF: **Immunological ignorance of solid tumors.** *Springer Semin Immunopathol* 2005, **27:**19-35.
13. Chen JJ, Lin YC, Yao PL, Yuan A, Chen HY, Shun CT, Tsai MF, Chen CH, Yang PC: **Tumor-associated macrophages: the double-edged sword in cancer progression.** *J Clin Oncol* 2005, **23:**953-964.
14. Bingle L, Brown NJ, Lewis CE: **The role of tumour-associated macrophages in tumour progression: implications for new anticancer therapies.** *Journal of Pathology* 2002, **196:**254-265.
15. Ingman WV, Wyckoff J, Gouon-Evans V, Condeelis J, Pollard JW: **Macrophages promote collagen fibrillogenesis around terminal end buds of the developing mammary gland.** *Dev Dyn* 2006, **235:**3222-3229.

16. Parsell DA, Mak JY, Amento EP, Unemori EN: **Relaxin binds to and elicits a response from cells of the human monocytic cell line, THP-1.** *J Biol Chem* 1996, **271:**27936-27941.
17. Dschietzig T, Bartsch C, Greinwald M, Baumann G, Stangl K: **The pregnancy hormone relaxin binds to and activates the human glucocorticoid receptor.** *Ann N Y Acad Sci* 2005, **1041:**256-271.
18. Deng WG, Zhu Y, Wu KK: **Up-regulation of p300 binding and p50 acetylation in tumor necrosis factor-alpha-induced cyclooxygenase-2 promoter activation.** *J Biol Chem* 2003, **278:**4770-4777.
19. Vane JR, Mitchell JA, Appleton I, Tomlinson A, Bishop-Bailey D, Croxtall J, Willoughby DA: **Inducible isoforms of cyclooxygenase and nitric-oxide synthase in inflammation.** *Proc Natl Acad Sci U S A* 1994, **91:**2046-2050.
20. Tsujii M, DuBois RN: **Alterations in cellular adhesion and apoptosis in epithelial cells overexpressing prostaglandin endoperoxide synthase 2.** *Cell* 1995, **83:**493-501.
21. Kim S, Takahashi H, Lin WW, Descargues P, Grivennikov S, Kim Y, Luo JL, Karin M: **Carcinoma-produced factors activate myeloid cells through TLR2 to stimulate metastasis.** *Nature* 2009, **457:**102-106.
22. Zeisberger SM, Odermatt B, Marty C, Zehnder-Fjallman AH, Ballmer-Hofer K, Schwendener RA: **Clodronate-liposome-mediated depletion of tumour-associated macrophages: a new and highly effective antiangiogenic therapy approach.** *Br J Cancer* 2006, **95:**272-281.
23. Rivas MA, Carnevale RP, Proietti CJ, Rosemblit C, Beguelin W, Salatino M, Charreau EH, Frahm I, Sapia S, Brouckaert P, et al: **TNF alpha acting on TNFR1 promotes breast cancer growth via p42/P44 MAPK, JNK, Akt and NF-kappa B-dependent pathways.** *Exp Cell Res* 2008, **314:**509-529.
24. Burow ME, Weldon CB, Tang Y, Navar GL, Krajewski S, Reed JC, Hammond TG, Clejan S, Beckman BS: **Differences in susceptibility to tumor necrosis factor alpha-induced apoptosis among MCF-7 breast cancer cell variants.** *Cancer Res* 1998, **58:**4940-4946.
25. Ewens A, Mihich E, Ehrke MJ: **Distant metastasis from subcutaneously grown E0771 medullary breast adenocarcinoma.** *Anticancer Res* 2005, **25:**3905-3915.
26. Kalluri R, Zeisberg M: **Fibroblasts in cancer.** *Nat Rev Cancer* 2006, **6:**392-401.
27. Robinson SC, Scott KA, Balkwill FR: **Chemokine stimulation of monocyte matrix metalloproteinase-9 requires endogenous TNF-alpha.** *Eur J Immunol* 2002, **32:**404-412.
28. Ismair MG, Ries C, Lottspeich F, Zang C, Kolb HJ, Petrides PE: **Autocrine regulation of matrix metalloproteinase-9 gene expression and secretion by tumor necrosis factor-alpha (TNF-alpha) in NB4 leukemic cells: specific involvement of TNF receptor type 1.** *Leukemia* 1998, **12:**1136-1143.
29. Leber TM, Balkwill FR: **Regulation of monocyte MMP-9 production by TNF-alpha and a tumour-derived soluble factor (MMPSF).** *Br J Cancer* 1998, **78:**724-732.
30. Shin SY, Kim JH, Baker A, Lim Y, Lee YH: **Transcription factor Egr-1 is essential for maximal matrix metalloproteinase-9 transcription by tumor necrosis factor alpha.** *Mol Cancer Res* 2010, **8:**507-519.
31. Richardson VJ: **Divergent and synergistic regulation of matrix metalloprotease production by cytokines in combination with C-C chemokines.** *Int J Immunopathol Pharmacol* 2010, **23:**715-726.
32. Hyc A, Osiecka-Iwan A, Niderla-Bielinska J, Moskalewski S: **Influence of LPS, TNF, TGF-ss1 and IL-4 on the expression of MMPs, TIMPs and selected cytokines in rat synovial membranes incubated in vitro.** *Int J Mol Med* 2011, **27:**127-137.
33. Hou CH, Yang RS, Hou SM, Tang CH: **TNF-alpha increases alphavbeta3 integrin expression and migration in human chondrosarcoma cells.** *J Cell Physiol* 2011, **226:**792-799.

Figure Legends

***Figure 1: E0771 breast cancer cells do not produce significant TNF-α* in vitro.**

By comparison, unstimulated RAW264.7, a transformed murine macrophage cell line, produces easily detectable TNF-α both when unstimulated and upon activation with 100 ng/mL LPS for 24 hours. Furthermore, cells separated from E0771 tumors using magnetic antibodies against CD11b (a surface marker for cells of myeloid origin and presumably including TAMs) also produced significant levels of TNF-α *in vitro*. ELISA sensitivity 5.1 pg/mL, n = 8 samples for all but E0771/CD11b^{+}, where n = 5. Both control (media only) and E0771 supernatants registered below sensitivity (not detectable).

***Figure 2: The E0771 cell line does not alter its TNF-α expression capability* in vivo**.

TNF-α is present in E0771 tumors grown in C57Bl/6 mice, but not mice lacking TNF-α. TNF-α levels quantified by ELISA as in Figure 1. Total protein levels quantified by BCA assay (n =7 per group). TNF-α sensitivity 5.1 pg/mL, and TNF-α$^{(-/-)}$ lysates registered below sensitivity (not detectable).

***Figure 3: E0771 does not respond by proliferating or apoptosing to TNF-α* in vitro.**

Proliferation of cells from all three lines (T47D, MCF-7, and E0771) treated with TNF-α is presented as fluorescent intensity of CyQuant DNA-binding dye standardized to the level of CyQuant fluorescence yielded by proliferation of an equal number of cells in untreated media , n = 10 per group. Pairwise comparisons indicate T47D proliferation is significantly ($p<.01$) elevated by 20 ng/mL TNF-α at 48 hours, while MCF-7 experiences significant ($p<.05$) decreases in proliferation at the same dose over the same time course. E0771 shows no significant alteration in proliferation in response to this dose over this time course.

Figure 4: Proliferation of macrophages* in vitro *is significantly and specifically impeded by ClodL therapy.

As in Figure 3, fluorescent intensities were standardized to the 0 mg/mL (media alone) condition for each group to account for differences in proliferative rate inherent to cell type. At all levels of ClodL, HFF-1 fibroblasts and E0771 breast cancer cells were unaffected and proliferated at a rate equivalent to those in PBSL, or in media alone, indicating that under these conditions ClodL is minimally active on these cell types. Only in the case of RAW264.7 macrophages did ClodL exert an anti-proliferative effect relative to PBSL controls, and did so in a roughly dose-dependent manner (n=8 each data point, $p<.05$ all points). The proliferation of RAW264.7 macrophages also was unaffected by PBSL therapy.

Figure 5: ClodL therapy strongly depletes F4/80^{+} TAMs in both wildtype mice and those lacking TNF-α.

Flow cytometry indicates that E0771 tumors grown in wildtype mice and TNF-$\alpha^{(-/-)}$ mice are partially comprised of TAMs that are sensitive to ClodL depletion. n = 21 wt/PBSL, 16 wt/ClodL, 15 TNF-$\alpha^{(-/-)}$ /PBSL, and 15 TNF-$\alpha^{(-/-)}$ /ClodL. These data also indicate that TNF-$\alpha^{(-/-)}$ animals do not exhibit baseline deficiencies in TAM recruitment to the tumor under control (PBSL) conditions relative to wildtype animals (p=.3496).

Figure 6A: Effects of macrophage depletion and TNF-α absence on SHG in the E0771 tumor.

The average brightness of SHG-producing fibers in tumors in wildtype/PBSL mice show significant elevation compared to other groups (p<.05), and tumors in wildtype/clodl mice show significantly decreased SHG compared to TNF-$\alpha^{(-/-)}$/PBSL tumors (p<.05). No other group was different from another (p>.05). n = 21 wt/PBSL, 16 wt/ClodL, 15 TNF-$\alpha^{(-/-)}$ /PBSL, and 15 TNF-$\alpha^{(-/-)}$ /ClodL.

Figure 6B: Effects of macrophage depletion and TNF-α absence on collagen IF in the E0771 tumor.

The average IF brightness of fibers in tumors in wildtype/PBSL mice shows a significant decrease compared to all other groups (p<.05). Tumors in TNF-$\alpha^{(-/-)}$/PBSL mice show significantly decreased IF compared to TNF-$\alpha^{(-/-)}$/ClodL tumors. No other group was different from another (p>.05).

Figure 6C: Effects of macrophage depletion and TNF-α absence on collagen I structure relative to total collagen I.

Tumors grown in wildtype/PBSL mice show significantly elevated OI relative to other treatment groups (p<.05). No other group was different from another (p>.05).

Figure 7: Lung metastatic burden decreases sharply with both macrophage depletion and TNF-α absence.

Tumors grown in wildtype/PBSL mice show significantly elevated metastatic output across ten sections of lung relative to other treatment groups (p<.05). No other group was different from another (p>.05). n = 21 wt/PBSL, 16 wt/ClodL, 15 TNF-$\alpha^{(-/-)}$ /PBSL, and 15 TNF-$\alpha^{(-/-)}$ /ClodL.

Figure 8: E0771 multiplicity decreases with TAM depletion or TNF-α absence, but the effects are not synergistic.

Tumor growth was measured by standardizing to tumor size at Day 3 (multiplicity) to minimize the possibility that slightly different numbers of cells may be injected even at constant injection volumes. Tumors grown in wildtype mice on PBSL therapy (n=21) are significantly larger than those grown in wildtype mice on ClodL therapy (n=16), at 27 days, as well as those grown in mice lacking TNF-α and exposed to either PBSL or ClodL (p<.05, n=15 both) at 27 days. None of the other three groups are different from each other (p>.05). No significant differences in multiplicity exist at earlier timepoints.

Supplementary Figure 1: Visualizing collagen I with SHG and IF.

This multiphoton microscope image is a composite of SHG (blue) and collagen I IF (red). Note that certain areas of a given fiber exhibit higher levels of SHG, and certain areas exhibit higher areas of IF, indicating that a given collagen fiber is structured differently at different areas along its length.

Supplementary Figure 2: Visualizing metastases with H&E staining.

This brightfield image of an E0771 metastasis in the lung of a wildtype C57Bl/6 female mouse clearly shows the hallmarks of separating cancer cells from normal lung cells: high ratio of hematoxylin (blue/violet) relative to eosin (magenta/red), surrounding abnormalities in lung structure, abnormal shape/size of nuclei and/or presence of abnormal mitotic spindles, and differences in cell shape and size.

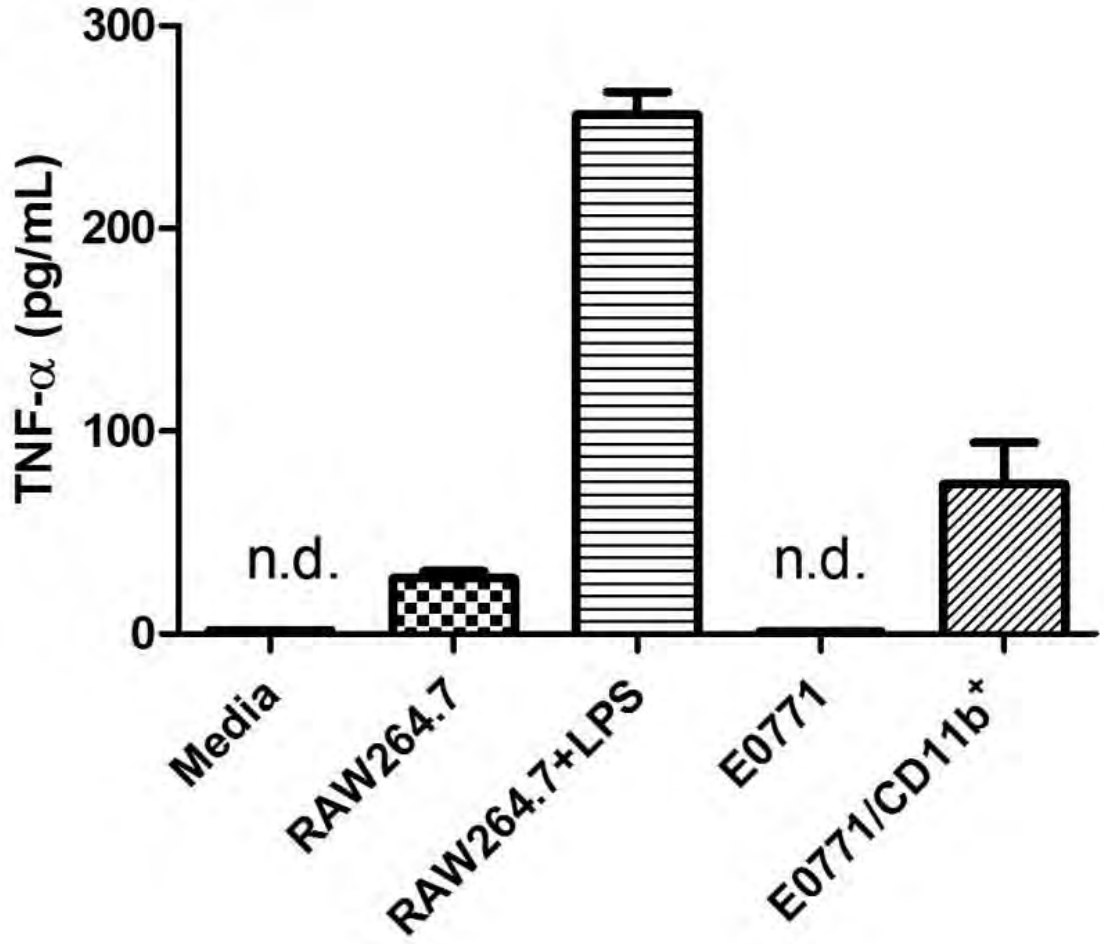
TNF-α (pg/mL)
300
200
100
0
n.d.
n.d.
Media
RAW264.7
RAW264.7+LPS
E0771
E0771/CD11b+

Figure 1

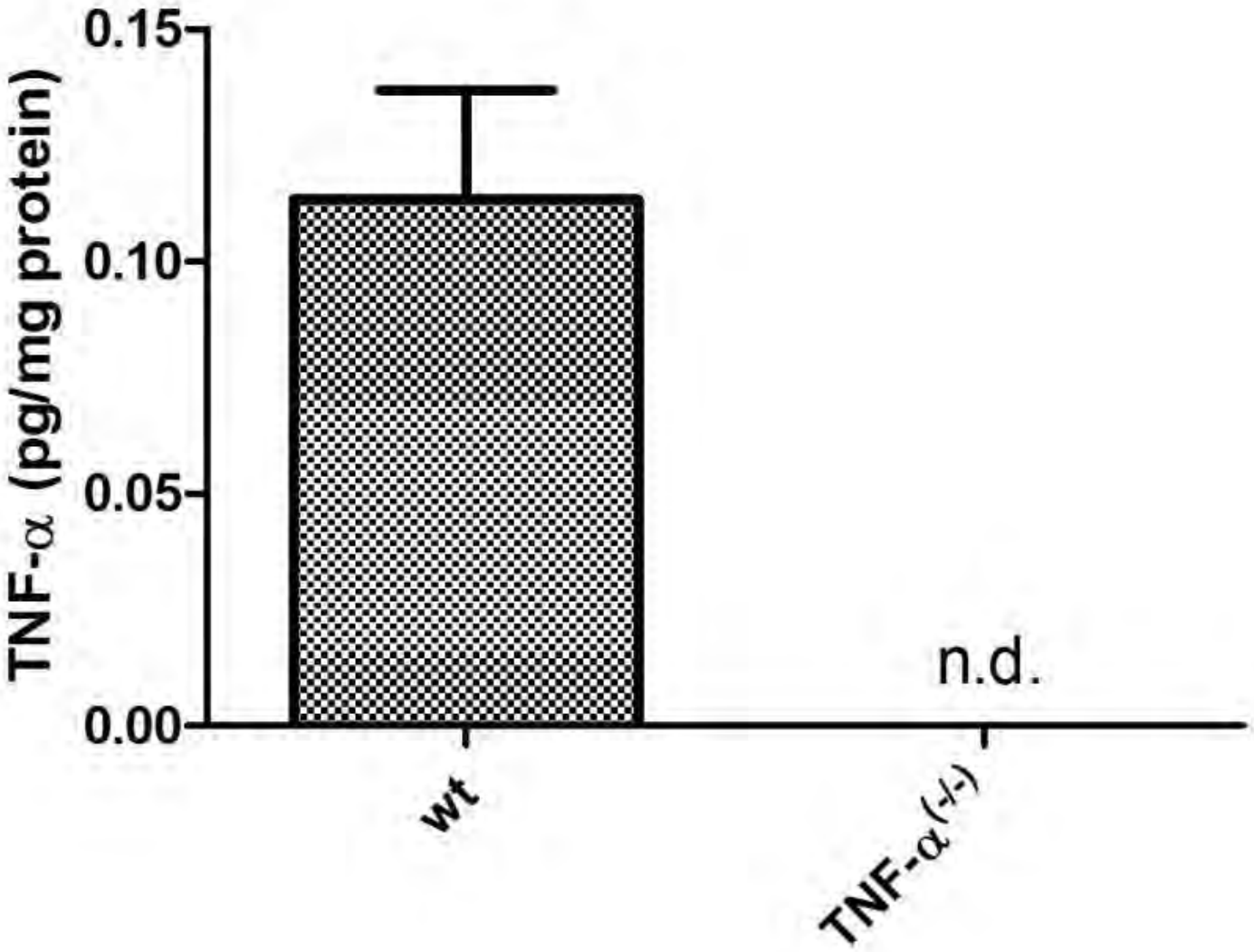

Figure 2

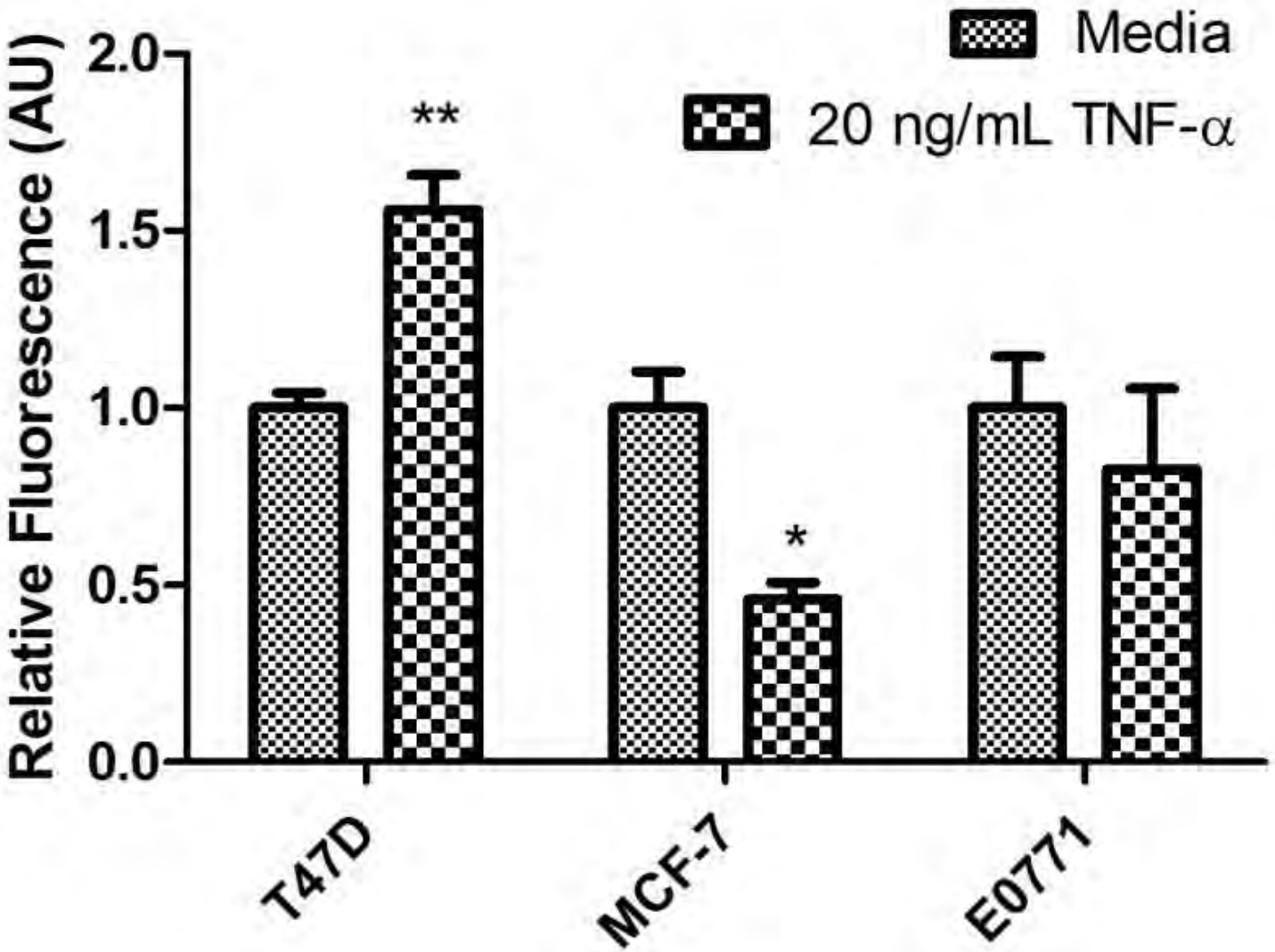
Media
20 ng/mL TNF-α
Relative Fluorescence (AU)
2.0
1.5
1.0
0.5
0.0
**
*
T47D
MCF-7
E0771

Figure 3

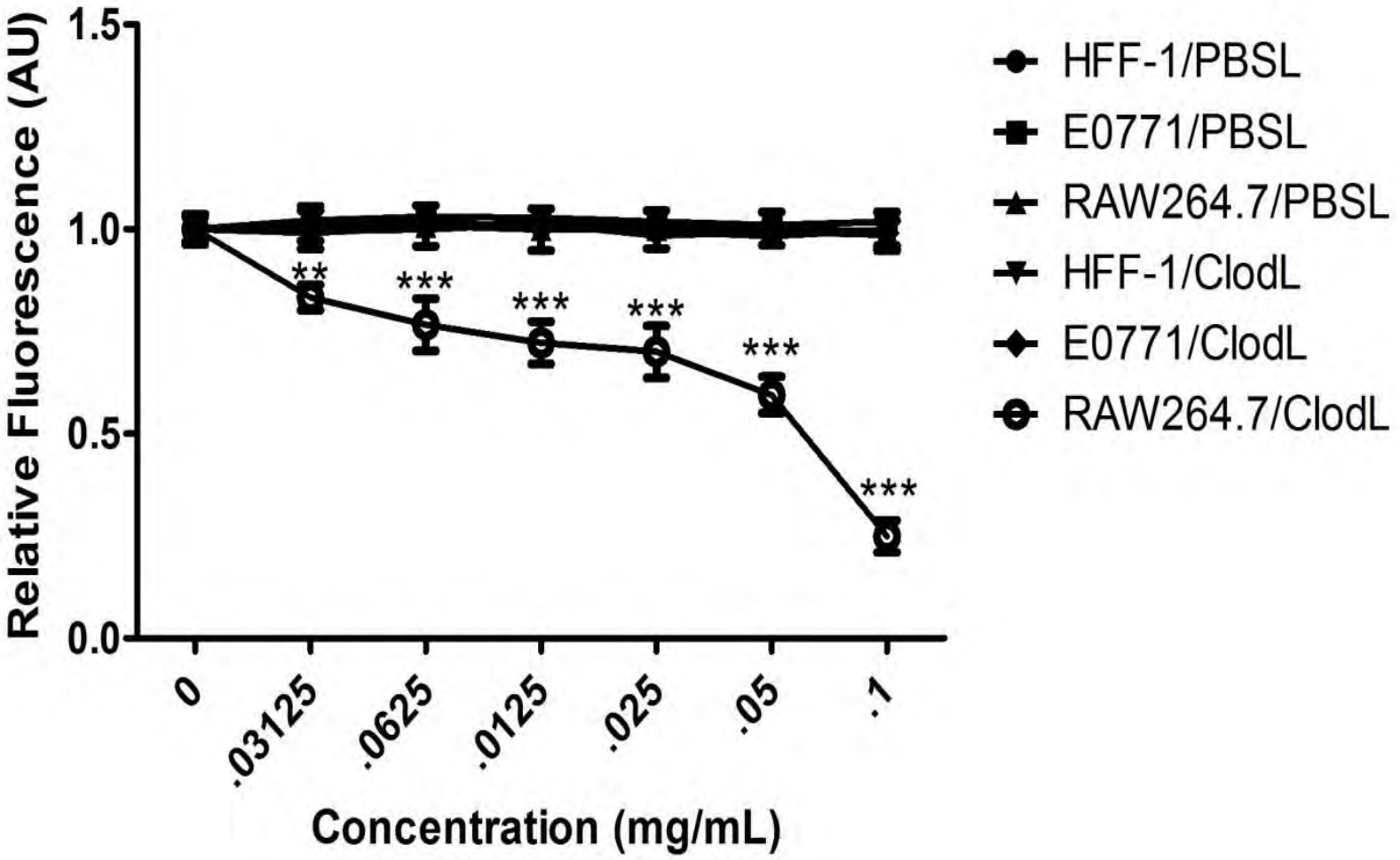
Relative Fluorescence (AU)
1.5
1.0
0.5
0.0
**
***
***
***
***
***
0
.03125
.0625
.0125
.025
.05
.1
Concentration (mg/mL)
HFF-1/PBSL
E0771/PBSL
RAW264.7/PBSL
HFF-1/ClodL
E0771/ClodL
RAW264.7/ClodL

Figure 4

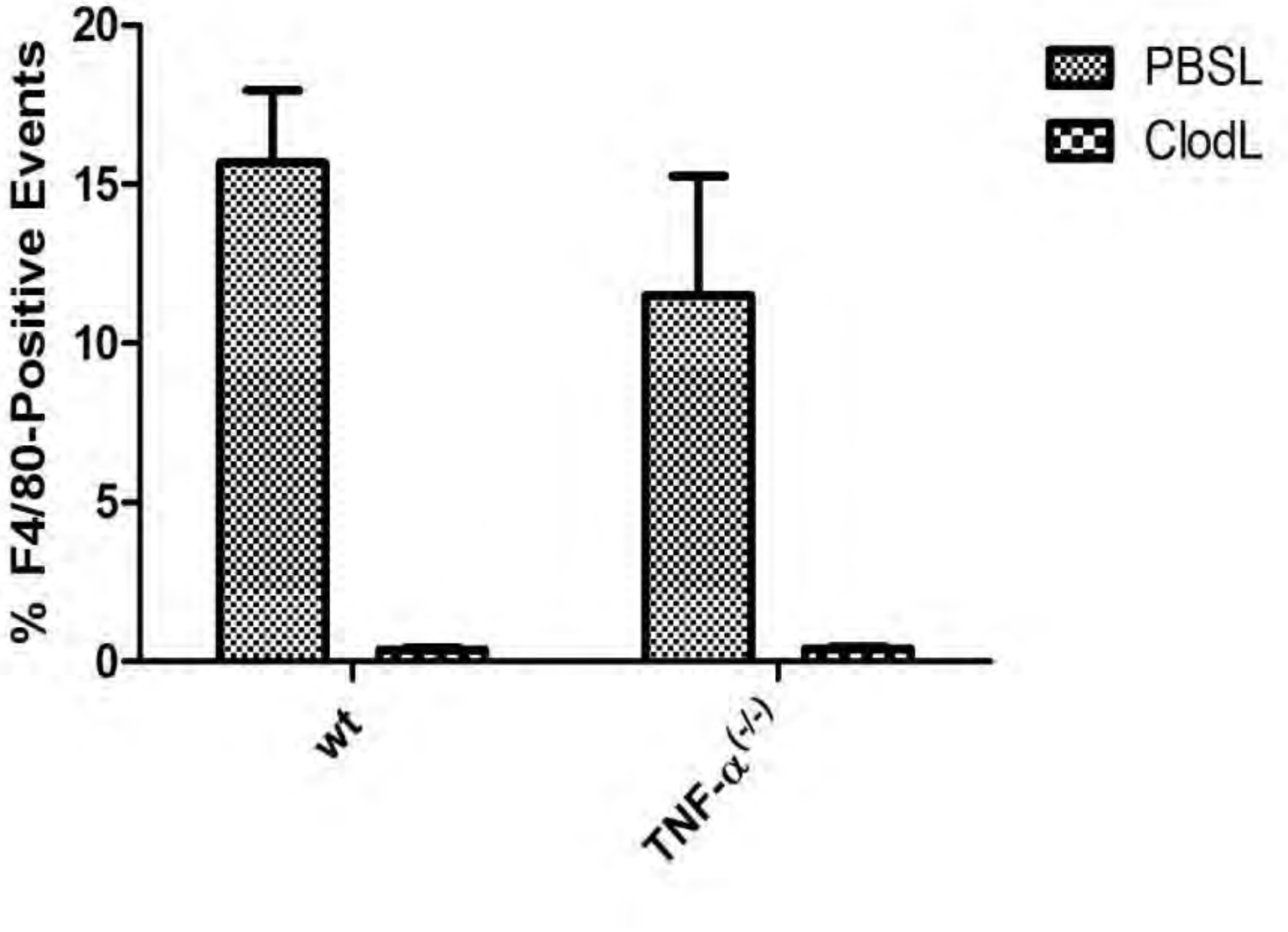

Figure 5

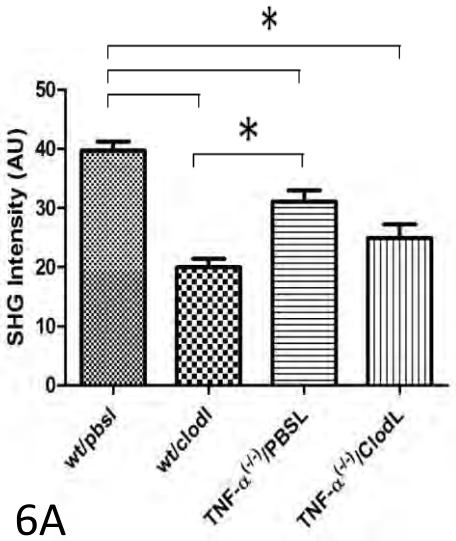

6A

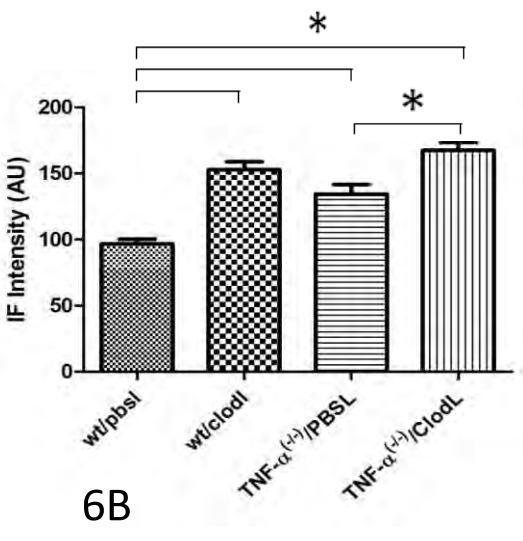

6B

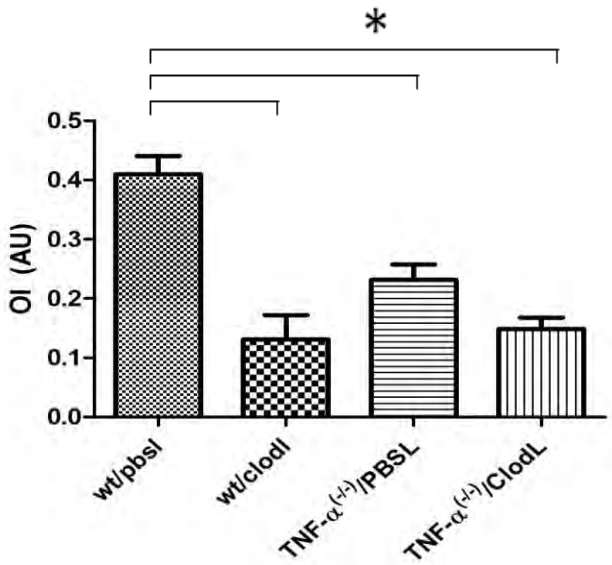

6C

Figure 6

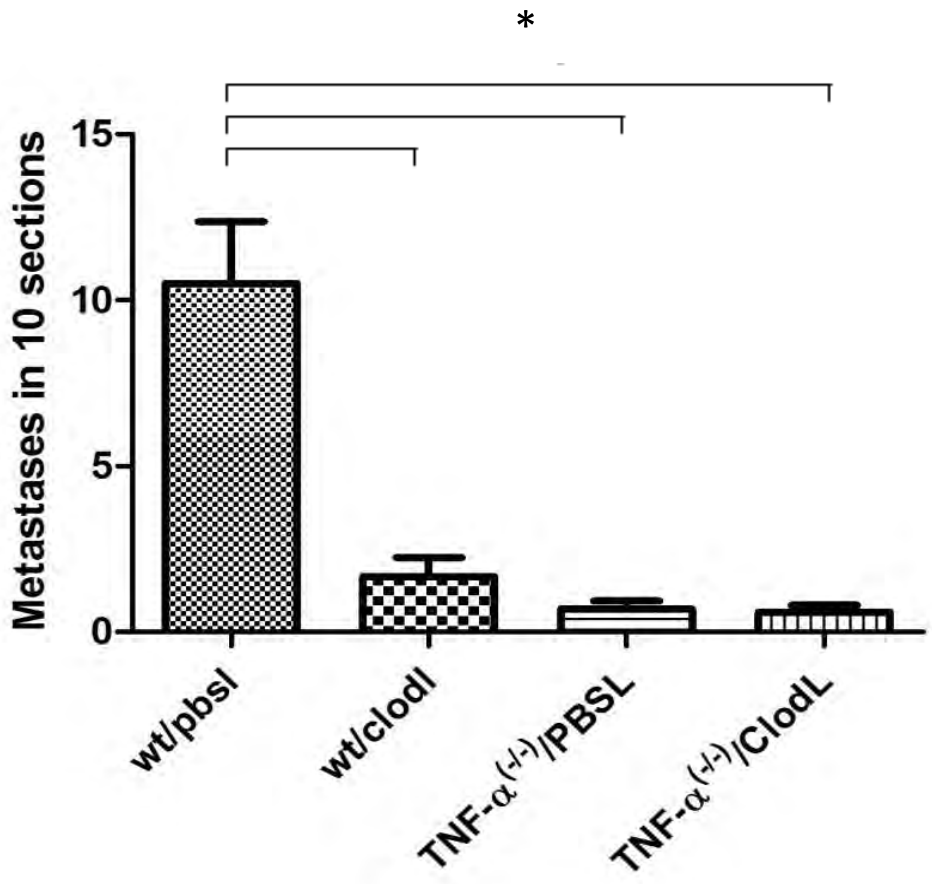
*
Metastases in 10 sections
15
10
5
0
wt/pbsl
wt/clodl
TNF-α(-/-)/PBSL
TNF-α(-/-)/ClodL

Figure 7

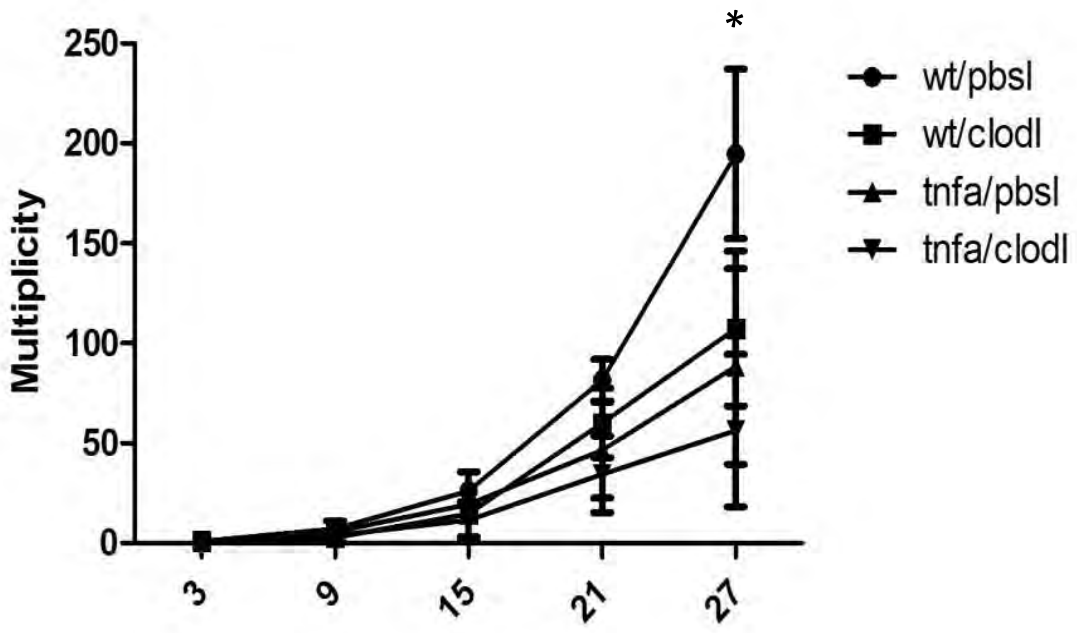
*
250
200
150
100
50
0
Multiplicity
3
9
15
21
27
wt/pbsl
wt/clodl
tnfa/pbsl
tnfa/clodl

Figure 8

Additional files provided with this submission:

Additional file 1: Supp1.pdf, 19K
http://breast-cancer-research.com/imedia/2040765668590442/supp1.pdf
Additional file 2: Supp2.pdf, 227K
http://breast-cancer-research.com/imedia/8170269505904427/supp2.pdf